EES Catalysis

REVIEW ARTICLE

View Article Online
View Journal | View Issue

Cite this: *EES Catal.*, 2024, 2, 475

Nanostructured single-atom catalysts derived from natural building blocks

Yajing Zhang, [ab] Guobin Yang,[ac] Jin Wang,[ad] Bin Zhao, [e] Yunxiang He *[ab] and Junling Guo *[abf]

Single-atom catalysts (SACs) exhibit maximized atomic utilization with individual metal atoms anchored on supporting materials, where the pursuit of high performance and low cost presents challenges. In this case, carbon provides structural versatility and customizable properties as a supporting material, which has been extensively studied. Biomass materials have emerged as promising precursors for the preparation of carbon-based SACs due to their renewable nature for sustainability, abundance for low cost, and high carbon content for advanced performance. In this review, representative synthesis strategies and advanced characterization techniques for biomass-derived CS-SACs are summarized, which facilitate the establishment of guidelines for the rational design and fabrication of biomass-derived SACs. In addition, we provide a timely and comprehensive discussion on the use of a broad range of natural biomass for SACs, with insights into the specific carbon nature of biomass resources, including their carbon structures, metal-carbon coordination environment, and center metal species. Furthermore, the application areas of biomass-derived CS-SACs in various catalytic processes are reviewed. Overall, the challenges and future perspectives of using biomass as precursors for SACs are outlined. We hope that this review can offer a valuable overview of the current knowledge, recent progress, and directions of biomass-derived SACs.

Received 6th November 2023,
Accepted 30th December 2023

DOI: 10.1039/d3ey00265a

rsc.li/eescatalysis

Broader context

Single-atom catalysts (SACs), particularly carbon-supported single-atom catalysts (CS-SACs), have arguably emerged as the most active new frontier in catalysis. Carbon support materials play pivotal roles in the development of CS-SACs. However, most of the precursors for these support materials are predominantly derived from non-renewable sources, and their synthesis usually requires harsh and energy-intensive conditions. Predictably, the utilization of synthetic precursors can also exacerbate serious social issues, including energy shortages, climate warming, and environmental pollution. In nature, carbon is coupled with other elements to give rise to a wide array of life forms, including plants, animals, and microbes. Thus, the use of carbon-based biomass sources as renewable precursors for the controlled synthesis of CS-SACs represents a sustainable alternative that has the potential to substantially reduce our reliance on fossil reserves and accelerate the sustainable advancement of human society. To accelerate the development of biomass-derived CS-SACs, it is necessary to summarize the recent progress on their design principles and biomass sources. This review aims to provide a comprehensive summary of recent advances related to the synthesis of biomass-derived CS-SACs, focusing on their synthetic strategies and many types of biomass precursors. Additionally, the remaining challenges and perspectives in the future of these emerging catalysts are further discussed.

[a] *BMI Center for Biomass Materials and Nanointerfaces, College of Biomass Science and Engineering, Sichuan University, Chengdu, Sichuan 610065, China. E-mail: yxhe@scu.edu.cn, junling.guo@scu.edu.cn*
[b] *National Engineering Laboratory for Clean Technology of Leather Manufacture, Sichuan University, Chengdu, Sichuan 610065, China*
[c] *Weihai Marine Organism & Medical Technology Research Institute, College of Marine Science and Technology, Harbin Institute of Technology, Weihai, Shandong 264209, China*
[d] *Pritzker School of Molecular Engineering, The University of Chicago, Chicago, IL 60637, USA*
[e] *Department of Bioproducts and Biosystems, School of Chemical Engineering, Aalto University, Espoo, FI-02150, Finland*
[f] *Bioproducts Institute, Department of Chemical and Biological Engineering, The University of British Columbia, Vancouver, BC V6T 1Z4, Canada. E-mail: junling.guo@ubc.ca*

1. Introduction

Single-atom catalysts (SACs) have emerged as a novel class of supported catalysts, which are characterized by catalytically active individual and isolated metal atoms anchored to suitable supports, enabling optimal metal utilization through the exposure of all metal atoms to the reactants and availability for catalytic reactions.[1–3] SACs have attracted substantial attention in recent years due to their unique properties, including exceptional catalytic activity, selectivity, and stability in reactions such as ammonia synthesis, oxidation, and hydrogenation. These distinctive properties arise from the low-coordination environment for metal atoms, quantum size effect, and strong metal–support interaction,

distinguishing them from traditional metal nanoparticles and mononuclear metal compounds.[4,5]

The support materials largely determine the catalytic performance of SACs. Extensive research has demonstrated that

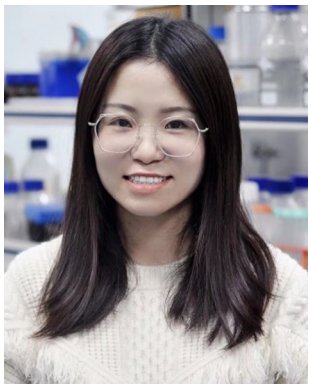

Yajing Zhang

Yajing Zhang received her Master's Degree from the Beijing University of Technology and is currently a PhD student in the Department of College of Biomass Science and Engineering at Sichuan University under the supervision of Professor Junling Guo. Her research interest is focused on the synthesis and application of organic/inorganic biohybrid materials based on metal-phenolic networks (MPNs) and further exploration of their interface chemistry.

Guobin Yang

Guobin Yang, a PhD student in the school of Marine Science and Technology at Harbin Institute of Technology, supervised by Professor Yanchao Wu. He is currently a visiting student at the BMI Center for Biomass Materials and Nanointerfaces at Sichuan University. His research focuses on the asymmetric synthesis of flavonoid polyphenolic skeletons and the synthesis and application of their functional derivatives.

Jin Wang

Jin Wang is a PhD student in the Pritzker School of Molecular Engineering at the University of Chicago. She was previously an undergraduate student at Sichuan University, where she worked at the BMI Center for Biomass Materials and Nanointerfaces. Her research focuses on bioelectronics and biomaterials.

Bin Zhao

Bin Zhao received his Master's Degree from Sichuan University and is currently a Doctoral student in the Department of Bioproducts and Biosystems (Bio2) at Aalto University under the supervision of Professor Orlando Rojas. His research interest focuses on developing advanced functional materials from plant biomass, highlighting their application in light management materials, including superblack materials, structure color, and CO_2 capture materials.

Yunxiang He

Yunxiang He received his PhD from the University of Bristol (UK) in 2019. He is currently an Associate Professor (Research) in the College of Biomass Science and Engineering at Sichuan University and the Platform Leader of Advanced Chemistry of the BMI Center for Biomass Materials and Nanointerfaces. His research focuses on polyphenol-functionalized polymers for biohybrid materials, which include the precise synthesis of polymers, polyphenol functionalization, and cellular behavior exploration. In addition, he is interested in the construction of novel functional biohybrid systems with inorganic materials.

Junling Guo

Junling Guo is an NSFC Excellent Professor and Director of the BMI Center at Sichuan University and Visiting Professor at The University of British Columbia. He received his PhD in Chemical and Biomolecular Engineering at The University of Melbourne and conducted his research at Harvard University as a Wyss Fellow. He has made numerous contributions to the field of polyphenol-based materials science, leading to the fundamental understanding of polyphenol chemistry and the development of new technologies for biomedical engineering, cellular engineering, carbon-neutral materials, and environmental technologies, among others.

the support materials not only provide strong stabilization for individual metal atoms but also play a crucial role in governing the local geometric and electronic structures of catalytic centers, resulting in exceptional retention of the isolated state and superior catalytic activity.[6–8] To date, single atoms have been successfully dispersed on a variety of support materials including metals,[9] metal oxides,[10] metal hydroxides,[11] sulfides,[12] phosphides,[13] zeolites,[14] and carbon-based materials,[15] enabling their widespread utilization as catalysts for thermochemical, electrochemical, and photochemical reactions.[16,17] Among the reported support materials, carbon is prevalent due to the advantages of high conductivity, high specific area, and abundant carbon reserves.[18–20] Furthermore, the structural diversity and designability of carbon-based materials (*e.g.*, amorphous carbon, graphite, and diamond) allow a regulatory structure–performance correlation for the understanding of the catalytic mechanism and the resulting SACs with desired performance.[21] In recent years, the precursors utilized for the synthesis of carbon-supported SACs (CS-SACs), comprising carbon and metal sources, have been elaborately designed but are limited by their complex structures and high production costs, including materials such as metal–organic frameworks (MOFs), covalent-organic frameworks (COFs), organometallic compounds, small molecular precursors, and functional polymers enriched with diverse heteroatoms.[22–30] Moreover, the preparation of synthetic precursors requires organic solvents and multiple chemical components, which not only hinder the further development of CS-SACs, but also aggravate serious social problems, such as the energy crisis, global warming, and environmental pollution.[31]

Although numerous synthetic CS-SACs have been proposed and explored, the research focus has shifted from synthetic materials to biomass from renewable natural resources as precursors for the preparation of functional CS-SACs. Compared to artificially synthesized organics, biomass in nature offers inherent merits, including a wide distribution, fine structures, diverse compositions, abundance, low cost, non-toxicity, ease of modification, and biodegradability, endowing it with great potential to be adopted as a sustainable source for carbon-based materials.[32,33] Owing to this fact, CS-SACs prepared from biomass are considered sustainable and environmentally friendly catalysts. To date, according to the different biomass sources, CS-SACs can be divided into raw biomass, waste biomass, and naturally biomass-derived chemicals. Firstly, the natural morphology and specific elemental compositions of raw or waste biomass precursors endow the derived carbon materials with very large surface areas, distinct porous structures, favorable electronic conductivities, and intrinsic receptiveness toward heteroatom doping.[34,35] Secondly, notably, natural biomass-derived chemicals (*e.g.*, macromolecules and small-molecule catecholamines) have increasingly been used as fundamental precursors for CS-SACs due to their diverse chemical structures and ease of modification. For instance, carbon-rich tannic acid (TA) and small molecules of dopamine have been employed for the preparation of precursors for CS-SACs based on the metal coordination properties of natural polyphenols.[36–38] Alternatively, cheap functional polysaccharides, such as chitosan and starch, as carbon sources, enable the gram-scale, pervasive synthesis of multifunctional CS-SACs.[39,40] The pursuit of utilizing naturally occurring materials, which are frequently regarded as ''green'' or ''sustainable'', presents a promising opportunity to broaden the range of carbon carriers for the fabrication of CS-SACs.

Given the fast development and increasing research interest in biomass-derived CS-SACs, a timely and comprehensive review is essential. In this review, we focus on the utilization of natural building blocks from a broad range of bio-resources to construct CS-SACs, emphasizing the significance of CS-SACs in addressing critical hurdles encountered in diverse catalytic applications (Fig. 1). Firstly, general synthetic strategies and representative advanced characterization techniques for biomass-derived CS-SACs are briefly introduced, followed by the detailed examination of the advantages and disadvantages of each synthetic strategy.

Subsequently, the natural building blocks from plants, animals, and microbes are introduced as precursors for the preparation of biomass-derived CS-SACs, including a discussion on their chemical composition, structural traits, catalytic performance, and inclusion in SAC design principles. In addition, by comparing the structure and function of natural building blocks and their potential for fabricating SACs, we provide some insights into the construction of biomass-derived CS-SACs and simply summarize their diverse applications at the present stage. Finally, we propose a short perspective on the current challenges and trends in the conversion of natural building blocks into SACs, which can further improve their utility in catalytic applications.

2. Synthetic strategies for biomass-derived CS-SACs

Challenges in the preparation of high-quality SACs are derived from the tendency of metal atoms to aggregate, which originates from the high surface energy of isolated single metal atoms on supports.[41–43] The foundational principles and rules for the fabrication of CS-SACs lie in the construction of intense interactions between a single metal atom and the carbon support.[44,45] Enormous efforts have been devoted to probing the various approaches for the fabrication of CS-SACs, where bottom-up and top-down methods are the two main categories with different integration modes of components.[46] In the case of bottom-up methods such as coprecipitation, atomic layer deposition (ALD), and wet chemistry synthesis, metal-containing precursors are adsorbed/anchored, reduced, and confined by defects on oxides or carbon supports with plenty of N or O defects or vacancies.[46,47] Alternatively, top-down methods (*i.e.*, pyrolytic carbonization) have shown promising perspectives for practical production and large-scale preparation in industry, where well-organized nanostructures can be further tailored and engineered with desired properties.[48–50]

As mentioned above, differing from synthetic carbon precursors, biomass materials have been increasingly acknowledged as

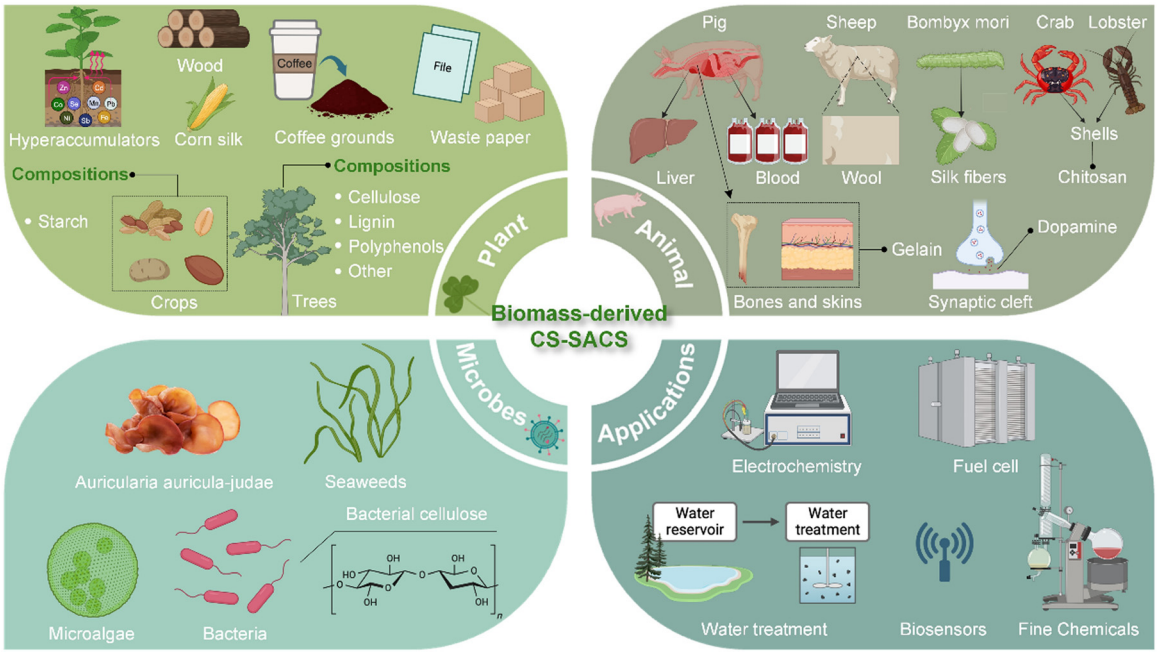

Fig. 1 Construction and versatile applications of CS-SACs using natural building blocks from natural biomass resources. Created with BioRender.com.

promising precursors for CS-SACs due to their affordability, widespread accessibility, and eco-friendliness.[33] In this section, we focus on the methods for preparing biomass-derived CS-SACs and their specific advantages/limitations (Table 1).

2.1 Carbonization strategy

Carbonization is the most straightforward and extensively used method for synthesizing atomically dispersed materials, which is achieved through the high-temperature decomposition of various precursors under a gas atmosphere (such as N_2, Ar, and NH_3).[89,90] This process can also be readily conducted in both laboratories and industrial factories. The biomass complexation strategy is a general approach for the preparation of catalyst precursors.[39] It is known that carbon is insufficient to prevent the aggregation of metal atoms due to its weak coordination with metal, which raises concerns in the synthesis of biomass-derived CS-SACs.

Heteroatoms are effective elements to stabilize isolated single atoms, typically, oxygen (O) and nitrogen (N) atoms. Accordingly, the oxygen-containing functional groups (*e.g.*, –OH and –COOH) in biomass can effectively adsorb metal ions *via* electrostatic interactions to impede their aggregation and well-confine the metal atoms.[91] N atoms have higher electronegativity and a similar atomic size as carbon (C), enabling their facile doping in N-poor biomass with internal or external N sources.[16] For example, *Spirulina* contains significant amounts of inherent protein, which can be used as natural nitrogen precursors to *in situ* generate N-doped biochar.[92] Also, the addition of external N sources such as urea, ammonium salts, nitric acid, melamine, and NH_3 gas during the carbonization process is commonly employed to incorporate N elements.[93] Moreover, besides O and N, phosphorus (P), sulfur (S), and chlorine (Cl) dopants have also been investigated to regulate the electronic structure of the active metal centers.[94,95] It is worth mentioning that certain trace elements of P, S, and Cl present in biomass can effectively serve as coordinating or neighboring moieties for metal atoms.[93,96] Du *et al.* employed reed bio-sorbent derivatives saturated with nitrate and sulfate to prepare Fenton-like catalysts for the decomposition of dinotefuran (DIN) by N and S co-

Table 1 List of synthetic strategies for biomass-derived CS-SACs

Synthetic strategy	Category	Advantage	Disadvantage	Ref.
Carbonization strategy	Direct carbonization	Using inherent metal elements of biomass; sustainable and green	Low metal loading	51–56
	Metal-salt-added carbonization	Tailoring different single metal centers; high metal loading	High cost	57–59
	Molten-salt-assisted carbonization	Much higher polarity; breaking chemical bonds; high yield	High cost; corrosive nature	60–73
	Other material-assisted carbonization	Adjustable microstructure; large-scale production	Dangerous etching reagent	74–85
Ambient synthesis	—	Low energy consumption and cost	Depending on the functions of precursors	86–88

doping, respectively, where S was doped in the crystalline Co_3O_4 phase due to the role of N as an anchor.[97] Compared to the S-free sample, the S-doped samples exhibited 1.71-times greater activity for the decomposition of DIN. Due to the different origins of biomass materials and synthetic routes and approaches, diverse as-prepared single metal atoms with different types of carbon supports can be produced, where the metal atoms are presented with well-defined coordination environments. Given that they naturally contain rich N and O heteroatoms, biomass-derived SACs generally present the M–N_4 and M–O_3C_1 configurations (Fig. 2). Different metal coordination configurations may lead to different performances in catalytic processes, which can assist in the selection of the carbon source for desired applications.

The complex chemical composition of biomass makes the thermal transformation process intricate, but control of the procedure allows the engineering of the resulting biomass-derived CS-SACs with desirable qualities and properties.[96] Based on the origin and carbonization environment of the biomass precursor in CS-SACs, this strategy can be classified into three categories, *i.e.*, direct carbonization, metal-salt-added carbonization, molten-salt-assisted carbonization, and other material-assisted carbonization.

2.1.1 Direct carbonization. Direct carbonization, using the inherent metal elements in biomass instead of adding external metal salts, opens up a sustainable and green strategy.[91] Interestingly, Fe is an essential element in biological systems, widely present in plant biomass, and capable of serving as an *in situ* catalyst.[51] For example, several biomasses such as *Enteromorpha*, *Spirulina*, and *Auricularia auricula-judae* possess a substantial organic iron content in their constituents, serving as an inherent metal source for the preparation of carbon-based Fe-SACs.[52–55] Additionally, utilizing biomass waste collected from phytoremediation offers an alternative for the *in situ* generation of SACs, which brings added advantages such as resource utilization and diminished potential for secondary pollution. For instance, by employing *Phytolacca americana*, an Mn hyperaccumulator, as the precursor, a novel Mn SAC featuring an Mn–N_4 structure was synthesized successfully through direct carbonization.[56] However, the majority of biomass mainly consists of C, O, and hydrogen (H), with typically low levels of intrinsic metal elements, which can potentially constrain the overall catalytic performance of the resultant CS-SACs.

2.1.2 Metal-salt-added carbonization. To overcome the constraint of the limited amount of metals in biomass, the approach of incorporating metal salts during carbonization has been extensively studied for the synthesis of biomass-derived CS-SACs.[91,96] Generally, metal atoms with different types in SACs show different catalytic behavior for various heterogeneous catalytic reactions.[57,58] Metal-salt-added carbonization enables the tailoring of different single metal centers, which can be rationally designed for the synthesis of functional biomass-derived CS-SACs. Besides, different types of metal atoms can be controlled by simply modulating the parameters in the synthesis process. For example, a series of SACs was developed by engineering bioinspired metal-lignin coordination complexes to atomically disperse transition metals (*e.g.*, Fe, Cu, Ni, and Co) in N-doped carbon.[59]

2.1.3 Molten-salt-assisted carbonization. Molten-salt-assisted carbonization, which employs a molten inorganic salt as the medium, has emerged as an important complementary route to the carbonization strategy for the synthesis of biomass-derived CS-SACs.[60–62] Despite the previously mentioned biomass complexation effect that can alleviate metal sintering to a certain degree, the eventual development of metal clusters or nanoparticles is unavoidable. Of course, these phenomena also explain why post-treatment procedures such as acid etching are used as a routine procedure in carbonization-based routes.[63] In this case, altering the carbonization environment, such as utilizing a special medium with strong polarity to interact with precursors, presents a viable approach to address this challenge.[64] Molten salts, a class of high-temperature solvents, are composed of free cations and anions, which can provide much higher polarity to break chemical bonds (including covalent, metallic, and ionic bonds) and suppress the aggregation of metal atoms.[64–66] Briefly, in the carbonization process, relying on the strong polarizing force, molten salts can release metal ions, allowing them to move freely, and eventually be captured by heteroatoms. More importantly, most spent salts can dissolve in hot water, making it easy to separate them from the product after carbonization.[67] Based on this, Wu *et al.* reported a facile one-pot strategy to directly transform raw pig liver biomass into porous CS-SACs with well-defined Fe–N_4 sites by high-temperature carbonization in bi-component NaCl/KCl molten salts.[62]

Besides the fundamental benefits outlined above, molten salt synthesis possesses other advantages compared to conventional solid-phase synthesis techniques, as follows: (1) the interaction between the molten salt and precursor enables better carbonization, leading to a significantly improved yield. (2) Molten salts possess a large heat capacity and thermal

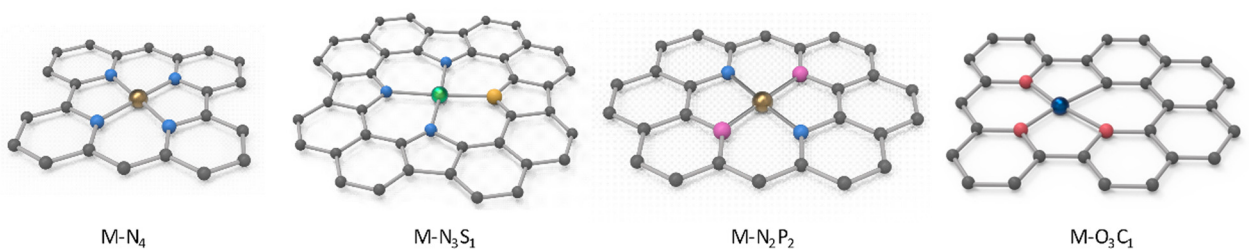

Fig. 2 Representative coordination environments of as-prepared CS-SACs derived from biomass materials.

conductivity coefficient, promoting the controllable and fast formation of desired structures. (3) Molten salts are stable in a wide temperature range, which can be continuously adjusted from approximately 100 °C to more than 1000 °C.[64,68,69] However, this strategy also presents certain challenges[70] such as the spent salts are not always easily dissolved and removed by simple treatment, such as hot water. For example, carbonate salts tend to solidify to rock-like hardness after carbonization.[71] Another challenge is cost. As is known, the common low-melting-point molten salts often contain expensive Li_2CO_3, but the regeneration of these salts is neither easy nor cheap.[72] Moreover, the corrosive nature of many salts imposes specific demands on reaction equipment and leads to elevated expenses.[73] Therefore, it becomes crucial to conform to the necessity before employing molten-salt-assisted carbonization for the synthesis of biomass-derived CS-SACs.

2.1.4 Other material-assisted carbonization. Various types of expendable materials such as silicon dioxide (SiO_2),[74,75] tellurium nanowires,[76] cetyltrimethylammonium bromide (CTAB),[77] and metal hydroxides, oxides or sulfides (α-FeOOH nanorods, $Co(OH)_2$ and $Ni(OH)_2$ nanoplates, and MnO_2, ZnO, and ZnS nanorods),[78,79] have been widely used to construct unique morphologies and pore structures in CS-SACs. Among them, benefiting from its physical and chemical integrity even at high temperatures, SiO_2 is commonly employed as a template to prepare various biomass-derived CS-SACs with high catalytic activity. The SiO_2 protection method in terms of the barrier effect can stabilize metal nanoparticles/clusters mainly by decreasing the surface energy of the metal atoms, which is effective toward the stabilization of highly loaded SACs.[83] For example, to achieve atomic dispersion, He *et al.* modified flexible biomass hydrogels (*i.e.*, chitosan, gelatin, and agar) with two strategies to minimize metal aggregation (Fig. 3a).[80] In addition to ''headstream fixation'' by materials such as complexation agents (*e.g.*, phenanthroline (PM)), the other ''roadblocks'' are based on rigid templates, such as SiO_2 nanoparticles and Zn atoms. Moreover, based on its structural and morphological features, SiO_2 can often be incorporated as a core or porogen, improving the porosity of the obtained carbon-based material. Consequently, the obtained carbon aerogels show a complex porous network containing a myriad of mesopores with an average size of about 10 nm, which is consistent with the diameter of SiO_2.

Notably, the silica-protective-layer assisted strategy, using SiO_2 as a coating material, can facilitate the reaction of N atoms with metal atoms during high-temperature carbonization to preferentially form catalytically active $M–N_4$ sites.[84,85] Based on this, Hu *et al.* successfully formed a uniform amorphous SiO_2 shell around polypyrrole-coated carbonaceous nanofibers (CNF@PPy) *via* the base-catalyzed hydrolysis of tetraethyl orthosilicate (TEOS) (Fig. 3b).[81] As designed, the SiO_2 shell not only restricted the free migration of Fe species but also captured volatile gaseous compounds during carbonization, achieving the simultaneous optimization of both the surface functionalities and porous structures of CS-SACs. Meanwhile, the resultant catalysts exhibit a much-enhanced oxygen reduction reaction (ORR) activity in 0.1 M $HClO_4$ with a half-wave potential of 0.74 V (*vs.* RHE), together with superior long-term stability (Fig. 3c and d). Nonetheless, not every single atomic site present in CS-SACs contributes to their ORR activity. Generally, the atomic $M–N_x$ moieties located on the external surface of the catalyst exhibit a higher propensity to engage in the ORR. Subsequently, unlike the traditional silica-protective-layer assisted strategy, Deng *et al.* employed a silica-restricted diffusion strategy to first coat polydopamine nanospheres (PDAS) with a thin silica layer, followed by physically mixing with $FeCl_3$, finally obtaining Fe atoms all anchored on the outermost surface of the carbon nanospheres (CNS) (Fig. 3e).[82] In this strategy, Fe migrates across the silica shell by atomic exchange with silicon, which not only prevents the aggregation of Fe but also causes the Fe atoms to anchor on the surface. Obviously, these Fe-SACs showed excellent ORR activity with an onset potential of 0.98 V and an ideal $4e^-$ pathway.

Although unique advantages of SiO_2 have been explored to accelerate the fabrication of various biomass-derived CS-SACs, the process for the removal of SiO_2 often requires a toxic solvent such as sodium hydroxide (NaOH) and hydrofluoric acid (HF), causing a variety of safety concerns. In addition, during the removal process, careful consideration must be given to its potential impact on the structural integrity and retention of the active metal sites in the final structure.

2.2 Ambient synthesis

The ambient synthetic strategy is a special preparation method for the synthesis of SACs under mild conditions, which is limited by the functions of the precursors. The development of ambient temperature synthesis techniques is primarily attributed to the excessive energy consumption and high production cost associated with pyrolytic synthesis methods, particularly when employing synthetic materials as precursors. Recently, Qu *et al.* elaborately designed an ambient synthetic strategy to directly transform easily accessible bulk metals such as metal foam (*e.g.*, Fe, Co, Ni, and Cu) into SACs (M-SACs/GO, M = Fe, Co, Ni, and Cu) by the strong bonding from the surface dangling bonds of graphene oxide (GO) support (Fig. 4a).[86] This synthesis at room temperature employing bulk metals was used to fabricate a series of M-SACs/GO, demonstrating its generality to access a variety of functional SACs. Subsequently, Ma *et al.* demonstrated a simple but robust carbonization-free route to prepare Co SACs by *in situ* wrapping an electrocatalytically active porphyrin-based thiophene-sulfur site-containing covalent organic polymer (PTS-COP) shell around a highly conductive multiwalled CNT (MWCNT) core, followed by accurately anchoring single-atom $Co–N_4$ sites on the macrocyclic porphyrin structure (Fig. 4b).[87]

Considering that the aforementioned synthetic method cannot be applied to all transition metals including precious metals, Pedireddy *et al.* presented a nature-based facile method to prepare metal-based SACs (M-SACs, M = Fe, Ir, Pt, Ru, Cu, or Pd) in a single-step at ambient temperature, using the extracellular electron transfer capability of *Geobacter sulfurreducens* (GS) (Fig. 4c and d).[88] Among them, the scanning electron

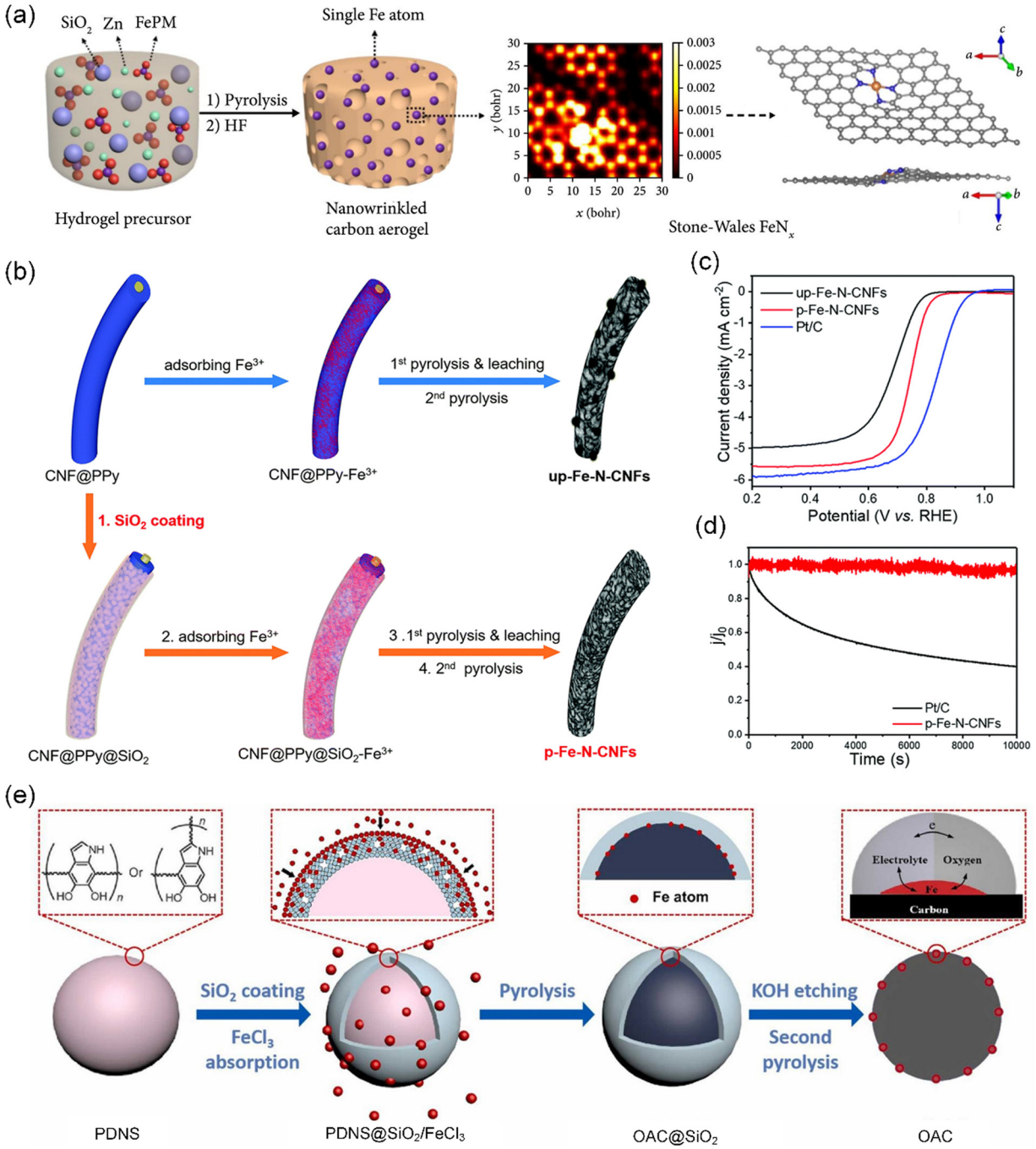

Fig. 3 SiO_2-assisted carbonization strategy. (a) Schematic representation of the synthesis of the NCA_{C-Zn}/Fe carbon aerogel. Reproduced with permission from ref. 80 (Copyright 2019, AAAS). (b) Schematic illustration of the fabrication of up-Fe–N-CNF (top) and p-Fe–N-CNF (bottom) catalysts. (c) Linear sweep voltammetry (LSV) curve of up-Fe–N-CNFs, p-Fe–N-CNFs, and Pt/C. (d) Chronoamperometric test of p-Fe–N-CNFs and Pt/C at 0.45 V *vs.* RHE. (b)–(d) Reproduced with permission from ref. 81 (Copyright 2018, The Royal Society of Chemistry). (e) Schematic illustration of the preparation of CNS with single Fe atoms at the triple-phase boundary. Reproduced with permission from ref. 82 (Copyright 2022, ScienceDirect).

microscopy (SEM) images of the representative Fe-SAC/GS displayed a crumpled morphology with many grooves on its surface, as shown in Fig. 4e, creating a high surface area for facilitating reactions. The transmission electron microscopy (TEM) image (Fig. 4e) and aberration-corrected high-angle annular dark-field scanning transmission electron microscopy (AC HAADF-STEM) image (Fig. 4f) both indicated the absence of detectable Fe clusters/nanoparticles on the surface of GS. Notably, the AC HAADF-STEM images distinctly revealed the presence of individual Fe atomic sites, as highlighted by a red circle in Fig. 4f, on the surface of GS. Similarly, merely altering the metal precursors can enable the preparation of M-SACs for various applications. Alternatively, Pedireddy *et al.* incorporated the ambient synthetic strategy in a biomass system,

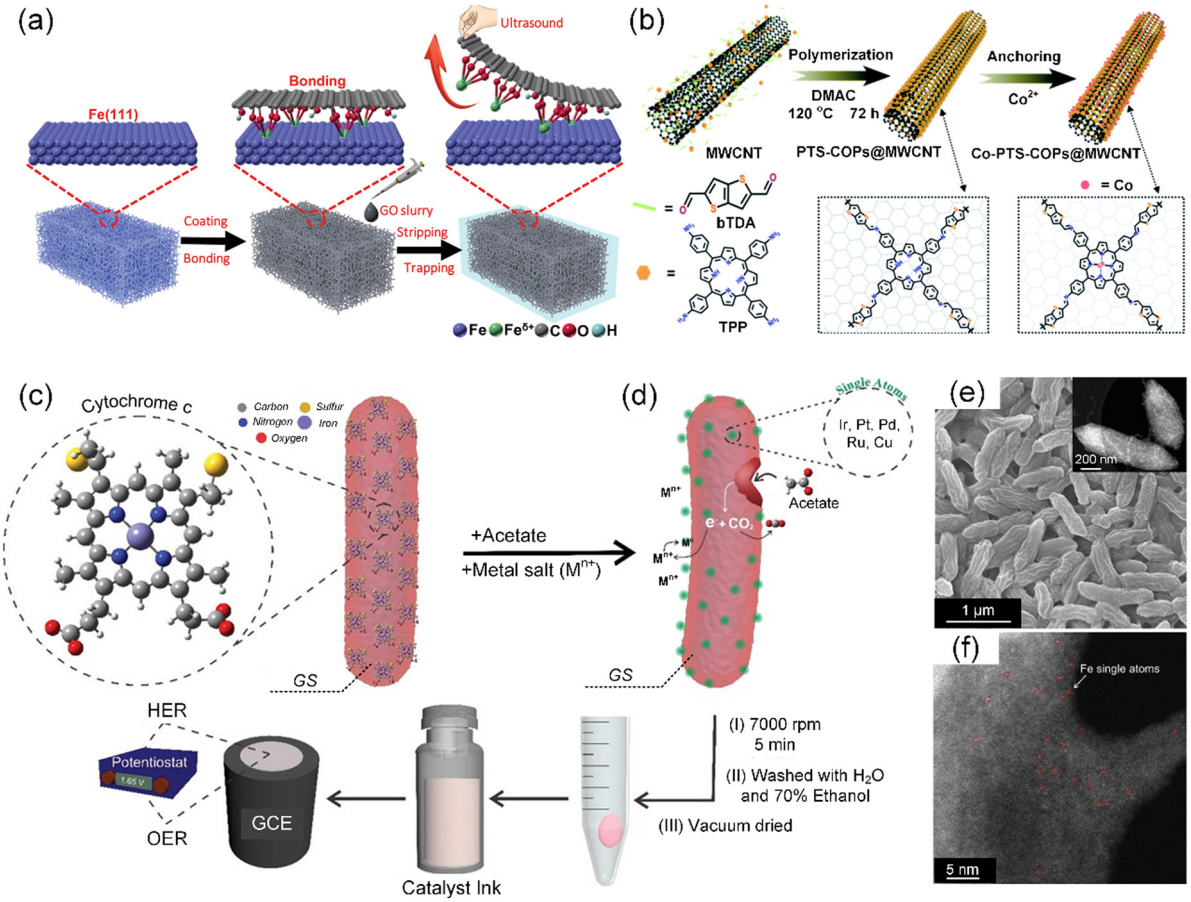

Fig. 4 (a) Schematic illustration of the preparation of Fe-SACs/GO. Reproduced with permission from ref. 86 (Copyright 2019, Wiley). (b) Schematic illustration of the carbonization-free synthesis of Co-PTS-COP@MWCNT hybrid. Reproduced with permission from ref. 87 (Copyright 2022, The Royal Society of Chemistry). Schematic showing (c) GS cell with expressed heme-containing c-type cytochromes (c-Cyts) on the outer membrane of the cell, which are responsible for the extracellular electron transfer to the acceptor moieties. (d) Mechanism for the reduction of the metal ions (electron acceptors) on the surface of GS cell membrane. (e) SEM image, with the inset showing the TEM image of Fe-SACs/GS. (f) AC HAADF-STEM image of Fe-SACs/GS. Individual Fe atoms are highlighted by red circles. (c)–(f) Reproduced with permission from ref. 88 (Copyright 2021, Wiley).

thereby extending the technique for the *in situ* synthesis of SACs from biomass sources.

3. Advanced characterization techniques for biomass-derived CS-SACs

The advancement of CS-SACs is also highly reliant on the application of sophisticated characterization techniques to conduct comprehensive investigations. After the preparation of CS-SACs, it is essential to identify both their geometric structure and electronic structure to validate their successful synthesis. To date, representative advanced analytical methods have been applied for the characterization of CS-SACs, such as spherical aberration-corrected high-angle annular dark-field scanning transmission electron microscopy (AC HAADF-STEM) and X-ray absorption fine spectroscopy (XAFS).[98,99]

3.1 AC HAADF-STEM

AC HAADF-STEM has a higher resolution compared to the conventional SEM or TEM techniques, enabling the clear characterization of sample microstructures with a resolution of 0.1 nm.[100] Consequently, this technique allows for the direct imaging of individual metal atoms dispersed on a support, which facilitates the identification of its precise location in relation to the surface structures and the determination of the spatial distribution of single metal atoms.[99,101] Currently, a variety of SACs (*e.g.*, Fe, Co, Ni, Cu, Zn, Mn, Pb, and Ru) has been identified by AC HAADF-STEM. Although AC HAADF-STEM has become the most persuasive and intuitive approach to assess the presence of CS-SACs, there are some intrinsic limits to using AC HAADF-STEM, which can only image a tiny part of samples and cannot identify the target element.[102] In particular, there are both single atoms and nanoparticles in as-prepared catalysts, while AC HAADF-STEM can miss key information due to the limited tested parts.

3.2 XAFS

In contrast to AC HAADF-STEM, XAFS is a special adjunct method that has been widely used to determine the local chemical structures of CS-SACs. Generally, XAFS can be typically

categorized into X-ray absorption near edge structure (XANES) and extended X-ray absorption fine structure (EXAFS) spectroscopy.[98,103] Specifically, XANES can reveal details about the electron and oxidation states, while EXAFS offers more information on the chemical bonding, interatomic distance, and coordination number of the target element by combining wavelet transform (WT) and Fourier transform (FT)-EXAFS analysis.[89,104] Different XANES adsorption curves often show the central atoms with different coordination numbers or ligands, making it easy to identify SACs. Alternatively, XAFS can also be used *in situ*/*operando* to provide significant insights into the structural evolution of SACs under real catalytic conditions.[102] This technique enables the monitoring of the dynamic electronic and local coordination structures of SACs during reactions. For example, *in situ* XAFS spectroscopy was performed during the ORR process to provide information regarding the successive structural transformations from Cu–N_4 to Cu–N_4/Cu-nanoclusters (NC), and then to Cu–N_3/Cu–NC, which reflected the change in the structure of the Cu SAS in its true electrochemical environment.[105] In summary, XAS and *in situ* XAS play a pivotal role in elucidating the atomic-level structural details of SACs, allowing for a deeper understanding of their reaction mechanisms.

Besides the above-mentioned methods, some other characterization methods can also provide additional information for CS-SACs, such as scanning tunneling microscopy (STM), X-ray photoelectron spectroscopy (XPS), energy dispersive X-ray spectroscopy (EDX), electron energy loss spectroscopy (EELS), X-ray powder diffraction (XRD), Fourier-transform infrared spectroscopy (FT-IR), and Raman spectroscopy. Moreover, density functional theory (DFT) calculations are often performed in conjunction with these characterization techniques for the structural detection of SACs. Considering the operational conditions of different instruments and the characteristics of SACs, it is essential to select appropriate characterization techniques.

4. CS-SACs from plant biomass

Plant biomass from trees, farm plants, and grasses is produced in huge quantities annually on a global scale and is an abundant renewable resource on Earth. Harnessing plant biomass, such as creating fires and building shields, is among the earliest wisdom of human civilization.[106] To date, advances in plant utilization have been explored in the fabrication of CS-SACs. In this section, the typical plant-derived biomass precursors for CS-SACs are summarized, including structural materials [wood, hyperaccumulators, solid biowaste (corn silk, spent coffee grounds, and waste paper)], saccharide-containing functional molecules (starch and cellulose) and aromatic compounds (lignin and polyphenols).

4.1 Structural materials

4.1.1 Wood. Wood is a natural, ubiquitous, and intrinsically renewable resource, with over three trillion mature trees on Earth serving as an important carbon sink during growth. Wood primarily consists of cellulose (30–50%), hemicellulose (15–35%), lignin (20–35%), and a portion of extractives.[107] Natural wood has a rich hierarchical micro-/meso-/macroporous structures and composed of well-oriented microfibers and tracheids for water, ion, and oxygen transportation during metabolism.[108] Due to its inheritable unique natural structure in the carbonization and activation processes, natural wood has been considered a promising precursor for the preparation of carbon materials with a regular morphology.[109,110]

Wood-derived carbon materials can directly use the natural porosity of wood to create channels and fabricate ''breathable'' carbon materials with the preserved mechanical strength and inherent microchannels of wood,[111] which inspires the preparation of SACs. Zhong *et al.* proposed a novel and effective strategy to form Fe-based SACs on plate wood-based porous carbon (Fe–N/WPC-SACs) in a two-in-one manner *via* a facile Lewis acid $FeCl_3$ pretreatment and subsequent carbonization process (Fig. 5a–d).[112] By using the Lewis acid $FeCl_3$, the two-in-one approach created microchannels (Fig. 5e) and incorporated atomically dispersed Fe–N active species (Fig. 5f) in the hierarchical structure during cell wall pretreatment. Chang *et al.* obtained a self-supported single-atom electrocatalyst with a macroscopic structure by anchoring atomically dispersed Ni single atoms (Ni SAs) on N-doped carbonized wood (Ni–N/CW-SACs) *via* a two-step successive carbonization process (Fig. 5g).[113] Benefitting from the NCW porous carrier (Fig. 5h), the Ni–N/WPC-SACs exhibited a high CO_2-to-CO faradaic efficiency (FE_{CO}) of 92.1% for CO production with a current density of 11.4 mA cm^{-2} at −0.46 V *vs.* RHE (Fig. 5i).

4.1.2 Hyperaccumulators. Hyperaccumulators are unique plants that can accumulate specific metals or metalloids in their living tissues to levels exceeding the normal levels of many plants by hundreds or even thousands of times.[114] To date, approximately 450 species of angiosperms have been recognized as hyperaccumulators of heavy metals, such as Cd, Co, Cu, Mn, Ni, Pb, Sb, Se, Fe, and Zn.[115] Thus, considering their ability to absorb heavy metals, many different hyperaccumulators have been employed for the remediation of metal pollution in soil, including *Elsholtzia splendens* and *Commelina communis* (Cu),[116,117] *Phytolacca americana* (Mn),[118] and *Arabis paniculata* (Pb).[119] However, the heavy metals in metal-rich hyperaccumulators may ultimately cause secondary contamination if released.[120] Some hyperaccumulators, particularly *Phytolacca americana* (*P. americana*) and *Myriophyllum aquaticum* (*M. aquaticum*), have been used as precursor materials for the preparation of CS-SACs and high-value utilization of biomass.

P. americana, originating from North America, was introduced in China in 1935 due to its ornamental and medicinal applications.[121] Unfortunately, it has become a present invader and has spread across China, especially in the central and southern regions.[122] Nevertheless, the ability to accumulate high concentrations of Mn, enables *P. americana* to be employed as a natural precursor for developing Mn-based CS-SACs. Cui *et al.* and Yang *et al.* successfully synthesized novel Mn-SACs *via* the *in situ* carbonization of the root and stem of *P. americana*, respectively.[56,123] The as-developed catalysts both

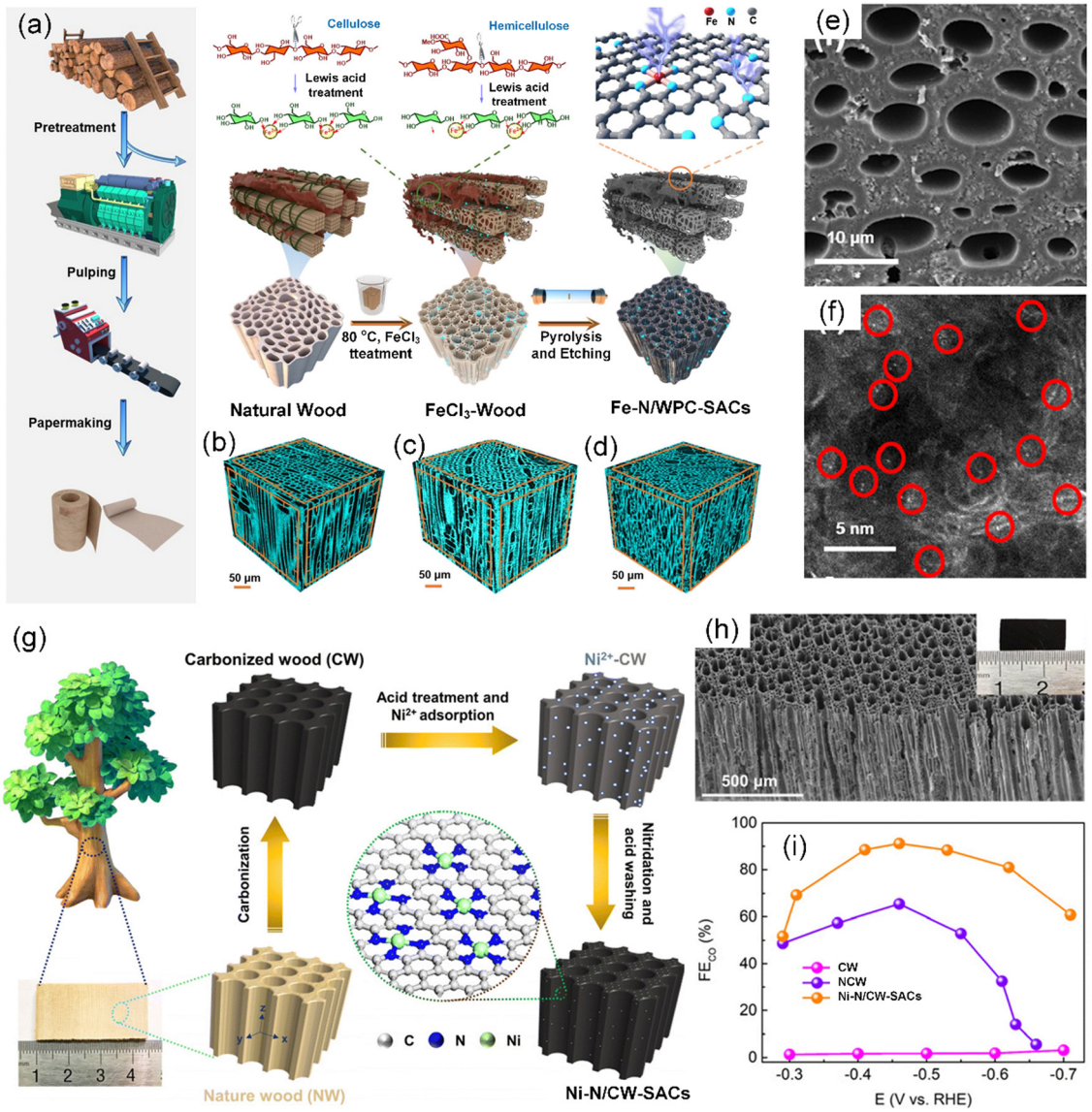

Fig. 5 (a) Schematic illustration of the procedure for the fabrication of Fe–N/WPC-SACs. Microscopic three-dimensional (3D) structure of (b) natural wood, (c) $FeCl_3$-wood, and (d) Fe–N/WPC-SACs. (e) SEM image of Fe–N/WPC-SACs. (f) AC HAADF-STEM image of Fe–N/WPC-SACs with the bright points representing Fe atoms. (a)–(f) Reproduced with permission from ref. 112 (Copyright 2021, American Chemical Society). (g) Schematic illustration of the preparation processes of Ni–N/CW-SACs. (h) SEM image of Ni–N/CW-SACs. Inset shows photograph of Ni–N/CW-SACs. (i) FE for CO production on CW, NCW, and Ni–N/CW-SACs electrodes at various applied potentials. (g)–(i) Reproduced with permission from ref. 113 (Copyright 2022, The Royal Society of Chemistry).

formed an $Mn–N_4$ structure, which could efficiently degrade and remove target organic pollutants, such as rhodamine B (RhB) and chloroquine phosphate.

M. aquaticum, a rooted emergent plant native to the Amazon River in South America, typically grows in freshwater streams, ponds, lakes, rivers, and canals.[124] This species has been one of the main aquarium plant introduced and sold in China for the past 20 years. *M. aquaticum* as an ornamental plant offers the benefits of wide distribution, rapid growth, and effective purification ability, which has been successfully employed in constructed wetlands for water treatment.[125] Recent studies demonstrated that *M. aquaticum* has potential to serve as a novel hyperaccumulator of Cd, demonstrating an enrichment capacity of 1.97 mg kg^{-1}.[126] Thus, considering its rich porous structure and abundant yield, Li *et al.* fabricated a novel *M. aquaticum*-derived Fe SAC *via* two-step carbonization, activation and graphitization, and chemical etching for peroxymonosulfate (PMS) activation to degrade organic pollutants.[127]

More strikingly, Fe-based SACs containing FeN_4 active sites were also successfully fabricated by utilizing Fe-contaminated fern biomass harvested from the phytoremediation of iron mines, which achieved a high degradation of antibiotic pollutants under natural mild conditions.[128]

4.1.3 Solid biowaste. Waste generation is increasing at an alarming rate as the global population and consumption patterns escalate.[129] Globally, 7–9 billion tons of waste is generated

annually, with about 1.3 billion tons reported to be municipal waste.[130] Depending on the disposal method, different types of waste can have different environmental and health impacts. However, the majority of solid biowaste is disposed in the environment through landfill or thermal incineration, which not only pollutes the air but also occupies valuable land resources.[131] Thus, considering environmental benefits and waste reuse, researchers have focused on converting these otherwise worthless solid biowastes, for example, corn silk, spent coffee grounds and waste paper, into high-value functional materials.

Corn silk, scientifically known as *Maydis stigma*, serves as a significant waste material from the production of maize crop and is usually collected and disposed as agricultural waste, manure, or animal feed.[132] Alternatively, as a biomass raw material, corn silk is mainly composed of carbohydrates, proteins, and vitamins, and has been regarded as an effective precursor for carbon materials due to its natural hollow microtubule structure and abundant micro-channels.[133,134] However, there are limited reports on the use of corn silk for the preparation of CS-SACs. It was shown that 3D corn silk-based porous carbon catalysts with dispersed Fe single atoms (Fe–N/CS-SACs) were developed for oxygen reduction/evolution reactions (ORR/OER) through the carbonization of corn silk with $ZnCl_2$, $Fe(NO_3)_3{\cdot}9H_2O$, and melamine (Fig. 6a).[135] In the simple strategy, $ZnCl_2$ and melamine play two crucial roles in removing the lignin to create numerous micro-/meso-pores and incorporating extra N element with an ultrahigh N content (10 wt%), respectively. The as-prepared catalysts demonstrated a high peak power density of 101 mW cm^{-2} (Fig. 6b) and maintained a stable discharge–charge voltage gap of 0.73 V for over 44 h (Fig. 6c), showcasing their strong potential for application in zinc–air batteries. The unique hollow tubular structures of corn silk provide more accessible active sites to promote the mass transfer of reactants (Fig. 6d–f).

Spent coffee grounds, the unutilized portion of the coffee beans left after the brewing process, tend to be discarded as solid waste without further utilization.[138] The production of instant coffee and coffee brewing produce about 6 million tons of waste coffee grounds worldwide annually, which is estimated to represent 50% of the input mass of coffee feedstock.[139] Even post-brewing, coffee grounds retain their inherent value as a valuable resource. Spent coffee grounds consist of significant quantities of organic compounds, including fatty acids, lignin, cellulose, hemicellulose, and various polysaccharides.[140] These compounds present an opportunity for extracting and producing valuable products with added value, such as a source of sugar, a precursor for activated carbon, and a sorbent for metal removal.[139] Spent coffee grounds have been reported to have a unique microporous structure with a high surface area of 300–1000 m^2 g^{-1}.[141] In particular, besides micronutrients, used coffee grounds also contain a high content of macroelements, *e.g.*, C, N, P, and K.[142] For the first time, Cui *et al.* obtained novel cobalt–carbon-supported SACs (Co-NS/CS-SACs) *via* the one-step carbonization of Co-soaked spent coffee grounds, in which Co atoms were anchored on the developed N/S-doped biochar (Fig. 6g).[136] The new type of SACs formed Co–N_3S_1 species *via* the coordination of Co atoms with N and S in the spent coffee grounds, exhibiting high efficiency in the activation of PMS to degrade various organic pollutants with a high efficiency of 90–100% (Fig. 6h and i).

Generally, waste paper refers to recovered paper, refused paper, scrap paper, secondary paper, discarded paper, used paper, and paper stock, which is a low-cost, renewable, and easily accessible material in daily life.[143] Furthermore, the increase in paper consumption generates a large amount of paper waste. Globally, the use of paper and cardboard produces over 100 million tons of paper waste annually.[144] Traditionally, waste paper, which typically contains 60–70% cellulose, plays an indispensable role in the circular economy as an essential alternative to wood and other plant-based fibers in the production of recycled paper. Currently, researchers have embarked on efforts aimed at developing multifunctional carbon-based materials from waste paper.[145,146] In particular, waste paper-derived active carbon (WPAC) can also be used as a low-cost and robust support to anchor Co atoms for the preparation of Co–N/WPAC-SACs due to its large surface area (535.2 m^2 g^{-1}) and abundant pore structures (Fig. 6j and k).[137]

4.2 Saccharide-containing functional molecules

Polysaccharides, as the largest component of biomass, are an important type of polymeric carbohydrate molecules constructed by joining monosaccharides through glycosidic linkages.[147,148] Estimably, more than 90% of carbohydrates in nature is found in the form of polysaccharides. As natural, nontoxic, and biodegradable polymers, polysaccharides are largely exploited from renewable biomass including terrestrial plants, animals, and microorganisms. Among the available biomass, plant polysaccharides are the predominant biomacromolecules in nature, with diverse roles including upholding the integrity of plant tissues as essential structural components (*e.g.*, cellulose, hemicellulose, and pectin) and serving as repositories of energy in the form of starch and fructans.[149] In the context of the circular economy, processing plant-derived polysaccharides has become a research opportunity. In this section, saccharide-containing functional molecules such as starch and cellulose in plant biomass will be introduced in the field of CS-SAC fabrication.

4.2.1 Starch. Starch, the stored form of carbohydrates, is manufactured by plants, and especially by crops in the form of granules in huge amounts.[150] The main characteristics of starch granules, such as their size, shape, structure, and chemical property, also depend on the corresponding botanical sources, including cereal starch, tubers starch, and legume starch. Starch mainly contains two distinct polysaccharide structures, *i.e.*, amylose and amylopectin.[151] In general, starches consist of approximately 20–30% amylose, 70–80% amylopectin, and other minor constituents such as lipids, proteins, and minerals.[152] Starch has long been regarded as an essential source of nutrition and energy for humans and animals, but also used for various purposes in the non-food industry sector, such as pharmacy and biotechnology nowadays.[153]

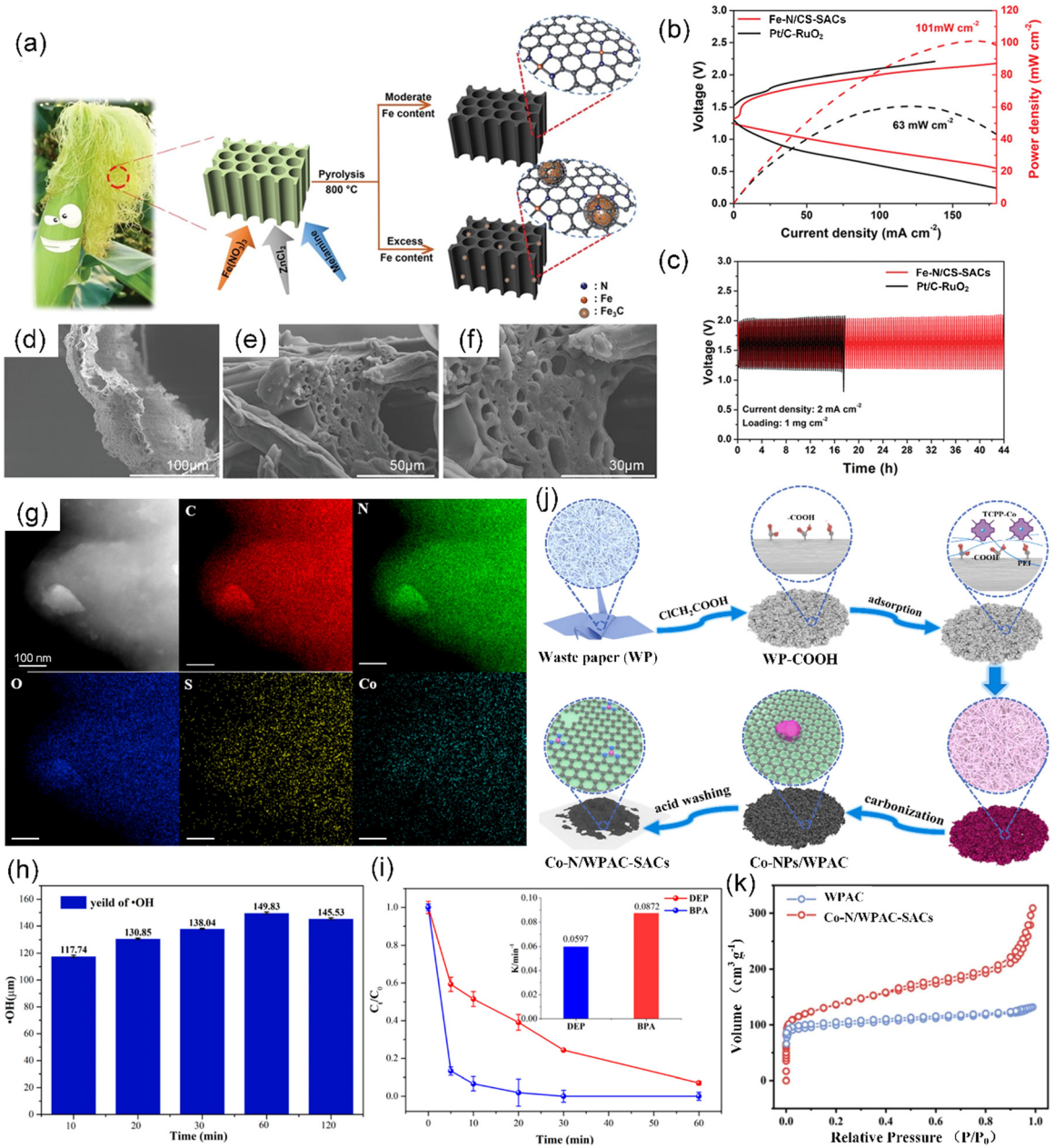

Fig. 6 (a) Illustration of the synthesis of Fe–N/CS-SACs. (b) Charge and discharge polarization curves of Pt/C–RuO_2 and Fe–N/CS-SACs air electrodes for a rechargeable Zn–air battery and the corresponding power density. (c) Cyclic stability at a current density of 2 mA cm^{-2}. (d)–(f) SEM images of corn silk. (a)–(f) Reproduced with permission from ref. 135 (Copyright 2023, Wiley). (g) Elemental mapping of Co-NS/CS-SACs. (h) Yield of ·OH in the Co-NS/CS-SACs/PMS system, using BA as a probe to quantitatively calculate the yield of ·OH. (i) Diethyl phthalate (DEP) and bisphenol A (BPA) degradation by PMS activated with Co-NS/CS-SACs. (g)–(i) Reproduced with permission from ref. 136 (Copyright 2021, the American Chemical Society). (j) Schematic illustration of the fabrication of Co–N/WPAC-SACs. (k) N_2 adsorption–desorption isotherms of Co–N/WPAC-SACs and WPAC. (j) and (k) Reproduced with permission from ref. 137 (Copyright 2023, ScienceDirect).

Recently, due to its high carbon content, renewability, and low cost, starch has been widely developed and broadly used as a desirable carbon precursor in the preparation of various advanced carbon materials.[154] For example, Cao *et al.* synthesized hierarchical porous carbon with a high specific surface area of approximately 2300 m^2 g^{-1} and controlled porosity as an electrode material for supercapacitors by employing biomass starch as the carbon source.[155] Hard carbon from starch was successfully prepared as an anode material for a sodium-based seawater battery, which exhibited an increased reversible capacity, current-rate capability, and cycling ability compared to commercial anodes.[156] Moreover, Wu *et al.* further utilized low-cost starch as a carbon source to develop isolated single-atom site metal/N and B co-doped porous carbon (M–NB/PC-SACs, M = Co, Fe, or Ni) catalysts with multi-functional catalytic performance *via* biomass-assisted carbonization-

etching-activation strategy (Fig. 7a).[40] In the *O*-silylation reactions, the M–NB/PC-SACs (M = Co, Fe, or Ni) exhibited excellent catalytic activity of approximately 99% conversion and nearly 100% selectivity (Fig. 7b). Remarkably, starch, an affordable starting material, can be employed in the large-scale production of M–NB/PC-SACs, thereby establishing the foundation for crafting, designing, and synthesizing specific SACs for industrial applications.

4.2.2 Cellulose. Cellulose, the primary structural component of plant cell walls, contains an abundant natural polysaccharide with the molecular formula of $(C_6H_{10}O_5)_n$ and is commonly found in trees and crops.[152,159] At the molecular level, cellulose is a type of linear polysaccharide formed by β-(1,4)-linked D-glucose units, exhibiting a flat ribbon-like conformation.[160] It is worth noting that the smallest physical structural unit of native cellulose is nanocellulose, which has a small diameter (typically less than 100 nm) and exhibits a high aspect ratio.[161] Nanocellulose can be further classified into three primary groups based on its cellulosic sources, processing conditions, and morphological characteristics including nanofibrillated celluloses (NFCs), cellulose nanocrystals (CNCs), and bacterial celluloses (BCs).[162] It was reported that up to 50% of the carbon element in plants is contributed by cellulose.[33] Cellulose has been widely employed as a biomass precursor to fabricate carbon materials,[163] especially as a desirable support for CS-SACs.

Carbonization is a common method to produce carbon materials from cellulose sources. Cellulose-derived Cu-SACs synthesized *via* simple one-step calcination displayed excellent catalytic activity and stability in the degradation of oxytetracycline.[164]

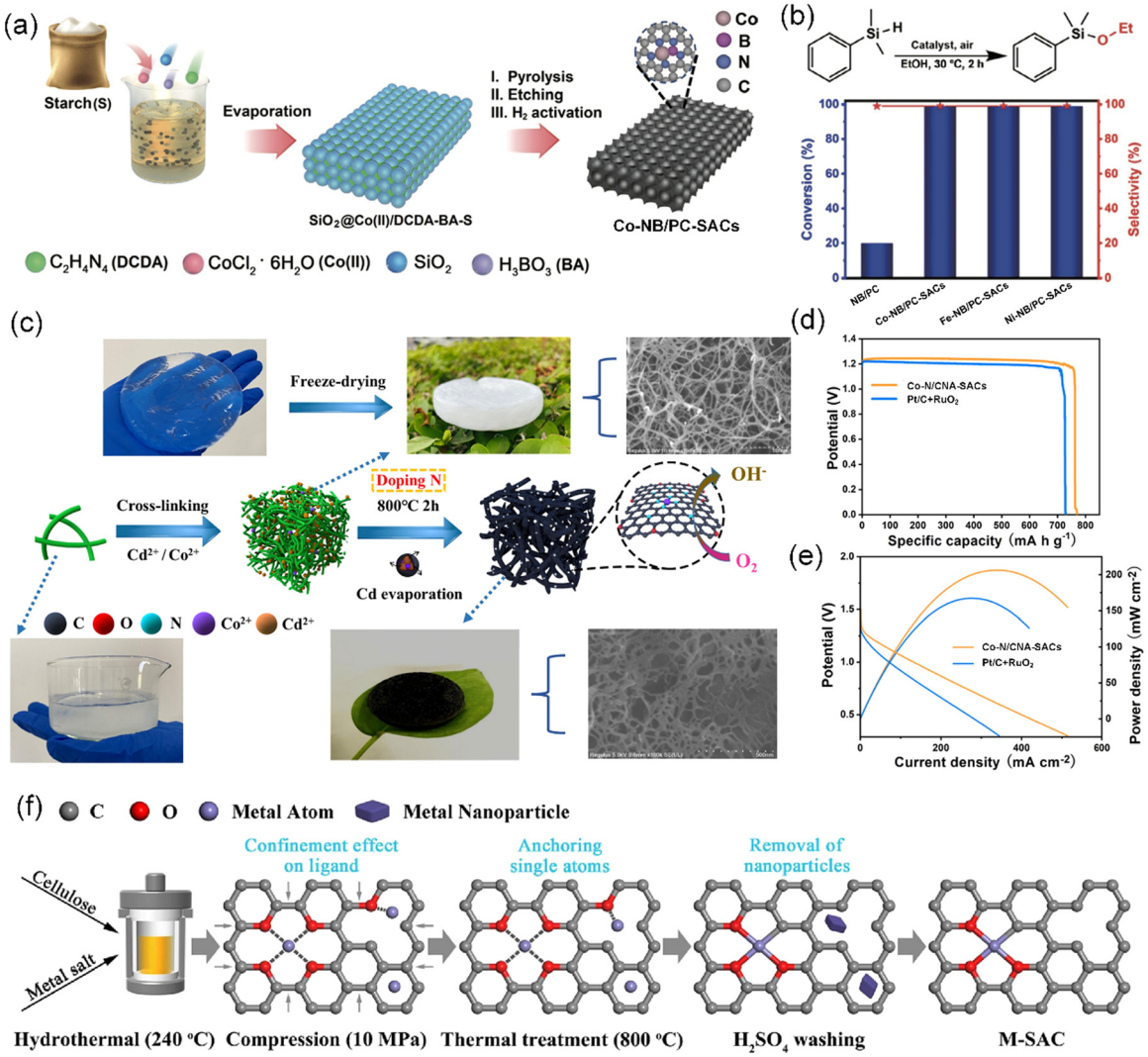

Fig. 7 (a) Schematic illustration of the biomass-assisted PEA approach for the preparation of M–NB/PC-SACs (M = Co). (b) Catalysis of the *O*-silylation reactions of dimethylphenylmethane in the presence of ethanol by different catalysts. (a and b) Reproduced with permission from ref. 40 (Copyright 2022, Springer Nature). (c) Schematic diagram showing the preparation of Co–N/CNA-SACs. (d) Galvanostatic discharge plots and (e) polarization/power density plots of zinc–air batteries with Co–N/CNA-SACs and Pt/C + RuO_2 air–cathode. (c)–(e) Reproduced with permission from ref. 157 (Copyright 2023, ScienceDirect). (f) Schematic diagram of the synthesis process of M-SAC. Reproduced with permission from ref. 158 (Copyright 2023, ScienceDirect).

It was revealed that the Cu-SACs showed a high dispersion of Cu atoms. The employed α-cellulose possessed a size of ~90 μm. Shen *et al.* effectively harnessed wood-based cellulose nanofibers (TOCNFs), which are rich in hydroxyl and carboxyl groups, to construct a TOCNF-Cd^{2+}/Co^{2+} complexation aerogel precursor, enabling the successful atomic dispersion of cobalt on N-doped carbon nanofiber aerogel (Co–N/CNA-SACs) after direct carbonization (Fig. 7c).[157] Cd salt facilitated the formation of a cross-linked aerogel, resulting in the generation of numerous internal micropores and defects, which in turn promoted the effective physical isolation of the Co atoms. Impressively, the as-designed Co–N/CNA-SACs not only showed superior ORR activity with the half-wave potential reaching 0.855 V but also a superior Zn–air battery performance with a high maximum power density (206 mW cm^{-2}) and impressive specific capacity (769 mA h g^{-1}) (Fig. 7d and e, respectively). In contrast to traditional carbonization methods, Li *et al.* introduced a novel approach that utilizes active O as anchoring sites and carbon from cellulose to obtain transition metal M-SACs (M = Fe, Co, Ni, Cu, and Zn) with a high metal content of 0.91–1.15 wt% through a combination of hydrothermal anchoring and compression confinement (Fig. 7f).[158] This was the first study achieving the direct synthesis of transition metal SACs from raw biomass, capitalizing on the ample carbon and active oxygen species, without introducing other heteroatoms.

4.3 Aromatic compounds

Aromatic compounds are chemical compounds made up of conjugated planar rings with delocalized π-electron clouds instead of single alternating double and single bonds. In plants, a wide variety of aromatic compounds can be found, while the most prevalent are phenolic compounds, which are present in various forms, including flavonoids, phenolic acids, tannins, stilbenes, and lignans.[165] Phenolic compounds, a class of chemicals with one or more hydroxyl groups attached to an aromatic ring, are ubiquitous secondary metabolites found in plant seeds, leaves, bark, and flowers, which have attracting increasing attention in recent years.[166] In this section, as aromatic-containing functional compounds, lignin and polyphenols are highlighted in the preparation of biobased CS-SACs.

4.3.1 Lignin. As a dominant aromatic chemical on Earth with an amorphous 3D structure, lignin is one of the major components of lignocellulose and widely exists in most terrestrial plant cell walls in the approximate range of 15% to 40% dry weight.[167,168] The main role of lignin is to fill the middle lamella of two adjoining cell walls, while also holding the cellulose fibril matrix together in the cell walls and providing plants with high mechanical strength.[32] Lignin is a complex cross-linked phenolic polymer formed by three primary units *via* dehydrogenation and radical polymerization, namely, *p*-coumaryl alcohol, coniferyl alcohol, and sinapyl alcohol, corresponding to the *p*-hydroxyphenyl (H), guaiacyl (G) and syringyl (S) structural units, respectively.[162,169,170] Notably, lignin is the only aromatic polymer with benzene rings in its building block with a phenylpropane structure among the three main components of lignocellulosic biomass.[171] In addition, the aromatic rings in lignin usually exhibit diverse functional groups, such as hydroxyl, benzyl, methoxyl, ether, and carboxyl, making lignin an appealing candidate for the development of numerous functional materials.[172] At present, most lignin sources are difficult to utilize due to their heterogeneity, and thus are usually used as fuels for energy supply in the pulping industry.[33]

Nevertheless, given its low price, high carbon content (>60%), and aromatic structure,[171] lignin can be transformed into a variety of carbon materials *via* controllable carbonization and activation processes, thus achieving value-added applications. For instance, Zhou *et al.* reported a universal synthesis method to produce SACs on N-doped carbon (M–N/CS-SACs, where M = Fe, Co, Ni, Cu) by carbonizing the phenolic complex of lignin coordinated with transition metal ions (Fig. 8a and b).[59] It was shown that lignin-based M–N/CS-SACs can effectively convert holocellulose-derived oxygenates into valuable building blocks and fragrance (Fig. 8c). The cleavage of C–N bonds is significant in organic and biochemical transformations, attracting considerable attention in recent years. Recently, a single Zn atom catalyst (ZnN_4-SAC), which was formed by the carbonization of a lignin alkali-coordinated single Zn complex, was found to be a robust heterogeneous non-noble catalyst, enabling the oxidative cleavage of C–N bonds in *N*-alkylamines and *N,N*-dialkylamines with the presence of O_2 (Fig. 8d and e).[173] These technologies not only offer a facile, cost-effective, and scalable approach for producing lignin-based CS-SACs but also pave the way for advancing the utilization of lignin and promoting the growth of the biomass economy.

4.3.2 Polyphenols. Polyphenols and polyhydroxyphenols mainly derived from plants are widely investigated due to their intrinsic chemical and biological properties, including biocompatibility, antioxidative capacity, anti-inflammatory effects, antimicrobial activity, metal ion coordination, and binding with biomacromolecules.[174] Plant-derived polyphenols are reported to be the fourth largest natural products after cellulose, hemicellulose, and lignin, and are also recognized as the seventh largest class of nutrients. To date, over 8000 polyphenolic compounds have been characterized and identified in whole plant-based foods, such as stilbenes, phenolic acids, lignans, and flavonoids.[175] Besides being highly abundant in nature, polyphenols exhibit a wide range of physical, chemical, and biological properties, which enable them to be used in the food, leather manufacturing, cosmetics, and pharmaceutical industries throughout history.[176,177]

Polyphenols consist of at least two hydroxyl groups and one or more aromatic rings. Common polyphenols usually contain dihydroxyphenyl (catechol) and/or trihydroxyphenyl (galloyl) groups. Particularly, catechol and/or galloyl groups can confer various covalent (*e.g.*, metal ion coordination) and non-covalent interactions (*e.g.*, hydrogen bonding, hydrophobic interactions, electrostatic interactions, π–π stacking and cation–π interactions) to drive the assembly of polyphenol-based materials (nanofilms, particles, and hydrogels) in multidisciplinary areas.[174,178] Among them, the coordination between polyphenols and metal ions stands out as one of the extensively studied topics. Multivalent metal ions can trigger the crosslinking of

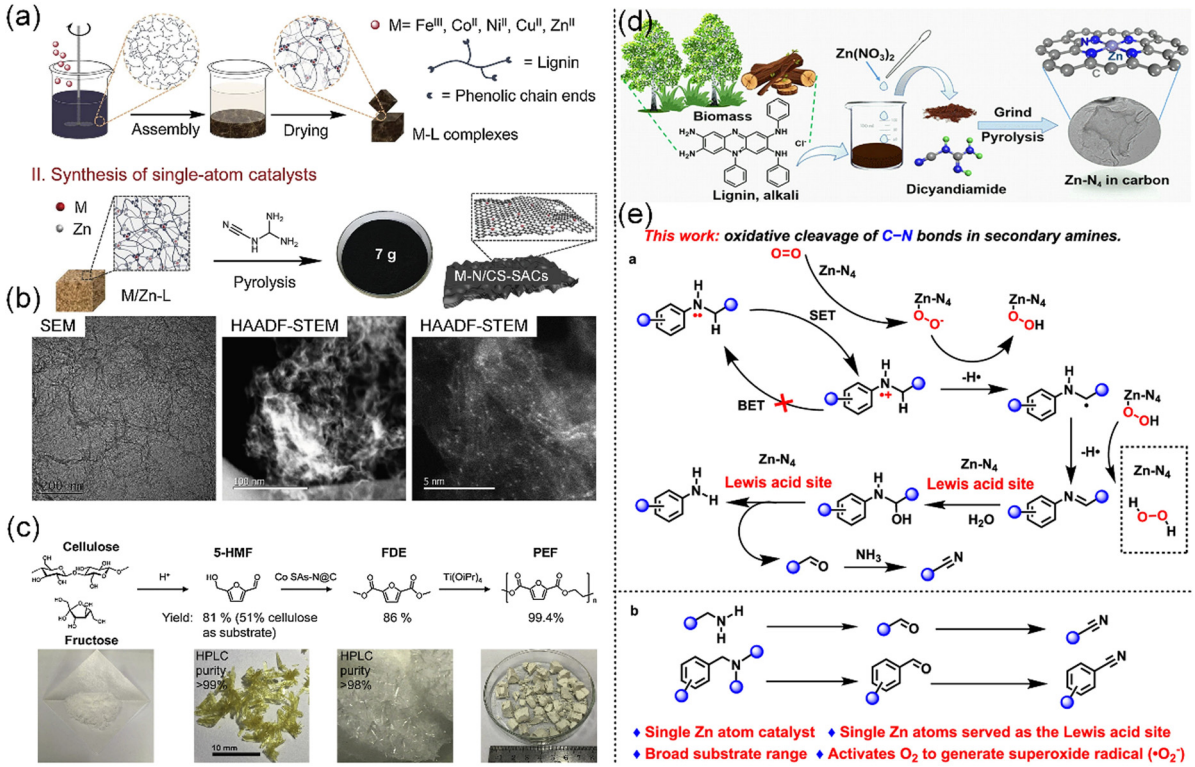

Fig. 8 (a) Strategy for the synthesis of M–N/CS-SACs. (b) TEM and HAADF-STEM images of M–N/CS-SACs. (c) Synthesis of polyethylene furanoate (PEF) from C6 sugars. 5-HMF: 5-hydroxymethylfurfural and FDE: 2,5-furandicarboxylic acid dimethyl ester. (a)–(c) Reproduced with permission from ref. 59 (Copyright 2019, ScienceDirect). (d) Procedure for the preparation of the ZnN_4-SAC catalyst. (e) Methods for the oxidative cleavage of C–N bonds in *N*-alkylamines in this work. (d) and (e) Reproduced with permission from ref. 173 (Copyright 2023, the American Chemical Society).

polyphenols without any assistance from heat, electricity, and special solvents, ultimately resulting in the formation of a class of metal–organic materials, *i.e.*, metal–phenolic networks, which are commonly referred to as MPNs.[179,180] Due to the universal adherent properties of polyphenols, MPNs can be applied as coatings on diverse substrates or interfaces regardless of their structures and shapes (Fig. 9a and b).[36,181,182] Of course, polyphenols and a variety of metal ions can also endow MPNs with different performance and functions (Fig. 9c).[183] Furthermore, the metal-driven coordination of phenolic moieties also facilitates the interfacial assembly of colloidal building blocks on the secondary substrates. This polyphenol-based modular approach provides a versatile platform for the construction of complex functional supraparticles,[184,185] therapeutically engineered cells,[186,187] and photo-driven biohybrids for chemical production.[188]

Polyphenols are promising precursors for the preparation of CS-SACs due to their rich catechol and/or galloyl groups in structure and low price. As one of the most abundant plant polyphenols, TA possesses a highly branched structure resembling that of an octopus, where a central glucose molecule is linked to ten gallic acid units through five diacetyl ester groups. (Fig. 9a).[37,181] It is the most widely used in CS-SACs because of the rich pyrogallol groups in its structure and low price. Owing to the absence of heteroatoms such as N element, metal–polyphenol complexes alone cannot be successfully converted into single atoms on polyphenol-derived carbon support.[189] Consequently, the introduction of external heteroatoms can assist the fabrication of CS-SACs derived from polyphenols.

A universal synthesis technique of TA-based SACs was developed through one-step carbonization in an NH_3 atmosphere, introducing external N heteroatoms, which is not limited to the substrate materials, dimensions, and sizes.[37] In this strategy, TA is initially crosslinked with formaldehyde to form a uniform TA-formaldehyde (TAF) coating on various substrates, followed by chelation with metal ions, enabling the preparation of mono- and bi-metallic SACs (*e.g.*, Co, Fe, Mn, Co–Mn, and Fe–Mn) on diverse substrates (*e.g.*, carbon, SiO_2, TiO_2, and MoS_2), dimensions (0D–3D), and sizes (50–5 cm) (Fig. 10a–e). In another example, novel covalently cross-linked poly(HCCP-TA-BPS) nanospheres (PSTA) with a tunable hollow structure were prepared by using hexachlorocyclotriphosphazene (HCCP), TA, and 4,4′-sulfonyldiphenol (BPS) as three comonomers, followed by further coordination of the unreacted catechol groups on TA with metal ions to obtain SACs with Co–N_2P_2 sites on N/P co-doped mesoporous carbon nanospheres with a small particle size (~50 nm) and high specific surface area (411.60 $m^2\ g^{-1}$) (Fig. 10f and g).[189] As expected, the PAST-Co-1000 catalysts designed in this manner demonstrated remarkable electrocatalytic ORR activities in 0.1 M KOH, including high current density (6.4 mA cm^{-2}), excellent durability after 10 000 continuous cycles (slight shift in half-wave potential of ~5 mV), and superior methanol tolerance (Fig. 10h and i).

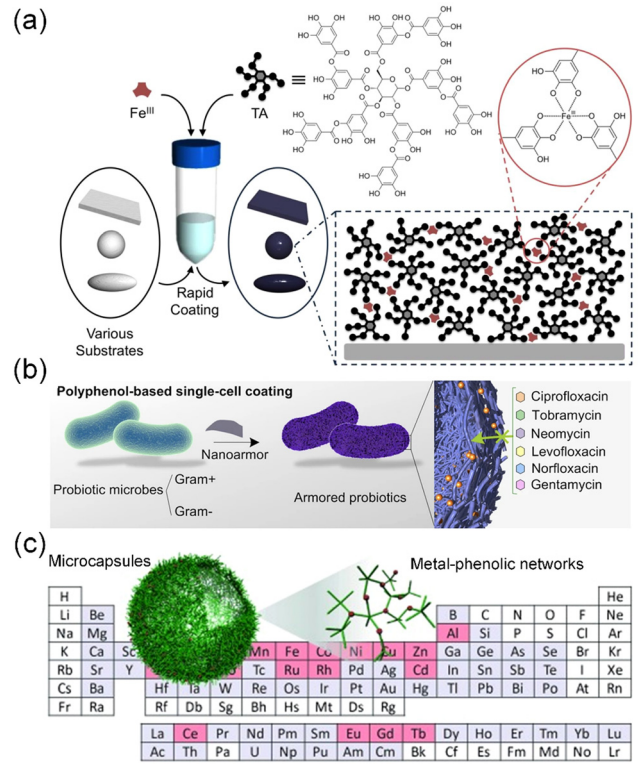

Fig. 9 (a) Schematic illustration of MPN assembly by coating TA–Fe coordination complexes on different templates. Reproduced with permission from ref. 36 (Copyright 2013, American Association for the Advancement of Science). (b) Nanoarmor formed by MPN-based single-cell coating enables rapid and highly biocompatible single-cell encapsulation. Reproduced with permission from ref. 182 (Copyright 2022, Springer Nature). (c) One-step assembly process utilizing TA can effectively coordinate diverse metals, resulting in the creation of a broad library of MPN capsules. Reproduced with permission from ref. 183 (Copyright 2014, Wiley).

Generally, plant-based precursors without doping mainly contain O as heteroatoms and can easily keep the original biomass structures in the final carbonized supports. Wood represents a hard biomass and contains a high content of crystalline cellulose, enabling the preservation of pristine structures and morphologies during carbonization. Sawdust and straws are the soft parts where the contained components are easy to hydrolyze into small pieces, further providing globular porous carbonaceous supports. High aromatic precursors such as lignin and polyphenols generally provide stable nonporous structures and a high degree of graphitization, while the cellulose and hemicellulose can undergo decomposition to afford abundant micropores due to the presence of abundant hydroxyl groups. Supports for CS-SACs can have tunable structures and designed properties by the selection of hard or soft plant sources with the corresponding components.

5. CS-SACs from animal biomass

There is an abundant variety of animals on Earth, which can provide biomass precursors for the synthesis of CS-SACs. Compared to plants, animal biomass as a raw material contains much more intricate compositions. In this section, several animal-derived biomass precursors used for the preparation of CS-SACs are summarized, including organ- or tissue-based materials (pig liver, pig blood, cocoon silk, and wool), macromolecular compounds (chitosan and gelatin) as well as small-molecule compounds (dopamine).

5.1 Organ- or tissue-based materials

5.1.1 Animal organs. Pig liver, a common animal organ found in pigs, is full of nutrients in protein, vitamins, and fat, with most of the fat being unsaturated, which is easy to add to the daily diet. Bioavailability is also an important aspect of protein. Thus, given its cost-effectiveness and rich protein content, pig liver, as a cheap raw biomass, is also used as a C and N source. For example, pig liver powder was thoroughly mixed with salt and $Fe(NO_3)_3$ by ball milling, which was carbonized at 800 °C under an N_2 atmosphere with the assistance of molten salt and converted into a porous CS-SACs with an atomic dispersion of Fe–N_4 active sites (termed Fe–N/CS-SACs) (Fig. 11a).[62] In the high-temperature carbonization process, the nitrogen species inherited from pig liver play a crucial role in capturing Fe atoms, thereby avoiding the formation of nanoparticles or clusters to a large extent.

Animal blood, particularly pig blood, represents one of the most common byproducts in the meat industry in the world. To the best of our knowledge, this blood is predominantly used as fodder or and thrown away as waste in slaughterhouses, seriously debasing its value.[194] It was noted that animal blood biomass contains a key component, namely, hemoglobin, which consists of four globular protein subunits joined by non-protein prosthetic heme groups.[190,195] Specifically, the large amount of Fe-porphyrin contained in hemoglobin plays an important role in forming Fe–N–C active sites for the synthesis of SACs.[191] Although Jiang *et al.* developed an efficient single atomic Fe–N–C electrocatalyst *via* the direct carbonization of pig blood inspired by the biological enzymes containing an Fe–N center,[196] there are still difficulties in manufacturing SACs directly from animal blood. The phosphorus lipids and polypeptides in animal blood constituting the cell membrane in blood cells, pollute the catalytic active site during the carbonization process, leading to a reduced performance due to the sintering of the active components.[191] Thus, it is important to remove the impurities from pig blood obtained in the initial slaughter before manufacturing CS-SACs through a direct carbonization process. Kim *et al.* prepared Fe-SACs dispersed on a hierarchically porous structure *via* a short heat treatment under NH_3 conditions after purifying waste pig blood with an organic solvent (acetone, hydrochloric acid, and toluene) (Fig. 11b and c).[190,191] Differently, in the carbonization process, Kim *et al.* added Zn salt as a sacrificial and activation template, while Lee *et al.* added additional thermal exfoliating graphene oxide with high porosity as a carbon support.

5.1.2 Animal tissues. Silk fibers (tens of microns in diameter), which are derived from *Bombyx mori*, show remarkable mechanical performance, high resilience, lustrous appearance,

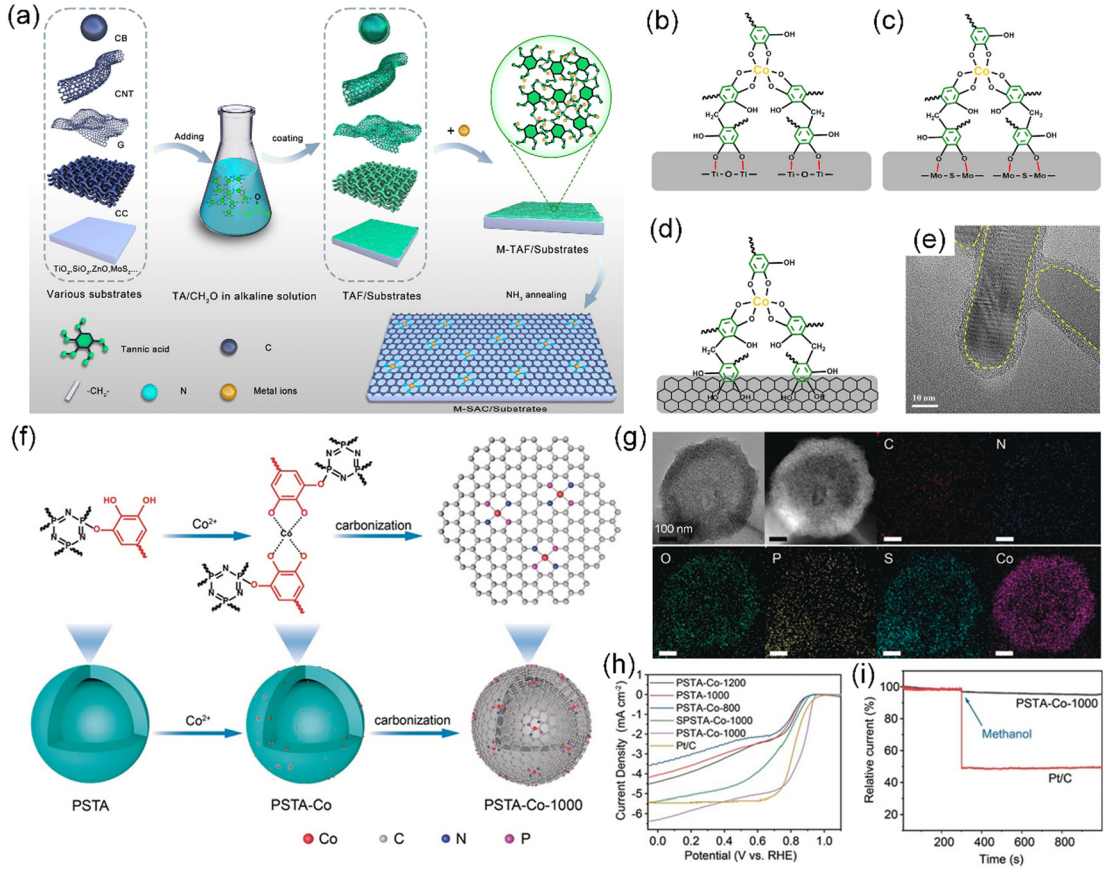

Fig. 10 (a) Process for synthesizing SACs on various substrates based on TA chemistry. (b)–(d) Proposed chemical structures of Co-TAF/TiO_2, Co-TAF/MoS_2 and Co-TAF/carbon, respectively. (e) TEM image of Co-TAF/TiO_2. (a)–(e) Reproduced with permission from ref. 37 (Copyright 2022, Wiley). (f) Preparation route to PSTA-Co-1000 hollow carbon nanospheres. (g) TEM image, HAADF-STEM image, and corresponding EDX element mapping of PSTA-Co-1000 nanospheres. (h) LSV curves of PSTA-Co-T (T = 800 °C, 1000 °C, and 1200 °C), PSTA-1000, SPSTA-Co-1000, and Pt/C at a rotating speed of 1600 rpm. (i) Tolerance to methanol by PSTA-Co-1000 compared with the Pt/C electrocatalyst, where the arrow indicates the injection time of methanol. (f)–(i) Reproduced with permission from ref. 189 (Copyright 2020, Wiley).

and large-scale production, and thus have been extensively utilized in the textile industry for thousands of years.[197] Due to the presence of amino-groups and the β-sheet configuration in silk fibroin, silk fibers have emerged as green and promising precursors for the production of N-doped two-dimensional (2D) carbon nanosheets through thermal treatment.[198] Zhu *et al.* developed a four-step cocoon silk chemistry strategy, including cocoon degumming, silk fibroin regeneration, salt-assisted carbonization, and acid etching, to synthesize SACs, which were embedded in ultrathin 2D porous N-doped carbon nanosheets (M–N/CN-SACs, M = Fe, Co, Ni) with a high N content (9.2 wt%) and large specific surface area (2105 $m^2\ g^{-1}$) (Fig. 11d).[192] In particular, the Co–N/CN-SACs demonstrated remarkable efficacy in activating C–H bonds, achieving a 68% conversion rate in the direct catalytic oxidation of benzene to phenol using hydrogen peroxide at room temperature (Fig. 11e and f). Wang *et al.* reported the synthesis of silk-derived 2D porous SACs with atomically-dispersed Fe–N_x–C (Fe-silk PN) and a large specific surface area (~2105 $m^2\ g^{-1}$) due to the strong interaction between Fe ions and amino groups and 2D lamellar structure of the regenerated silk fibroin.[198] The Fe-silk PNCs, prepared as described, exhibited an excellent electrochemical performance in the ORR, demonstrating a half-wave potential ($E_{1/2}$) of 0.853 V, remarkable stability with only 11 mV loss in $E_{1/2}$ after 30 000 cycles, and remarkable catalytic activity in OER.

Wool, a type of animal fiber, is mainly obtained by shearing fleece from living animals, such as goats. Wool fiber primarily consists of the animal protein keratin, which is a natural fiber rich in disulfide bonds.[193,199] Wool keratin has become a hot topic in recent years considering the regulation of the local coordination environment of SACs on their performance. For instance, Fe–S_1N_3 SACs embedded in ultrathin 2D porous carbon nanosheets were prepared from natural keratin through precise S and N coordination of the active center *via* a three-step wool keratin chemical strategy. The Fe–S_1N_3 SACs could be used for the oxidative degradation of organic pollutant substrates (MB, RhB, and phenol) (Fig. 11g–i).[193] The three steps in this wool keratin chemical strategy are as follows: (1) preparation of natural wool keratin, (2) addition of metal salts and carbonization and (3) acid etching.

5.2 Macromolecular compounds

5.2.1 Chitosan. Chitosan is mainly derived from the deacetylation of chitin, a type of linear polysaccharide polymer found in crustacean shells, *e.g.*, crabs and shrimp.[33,200] It is the

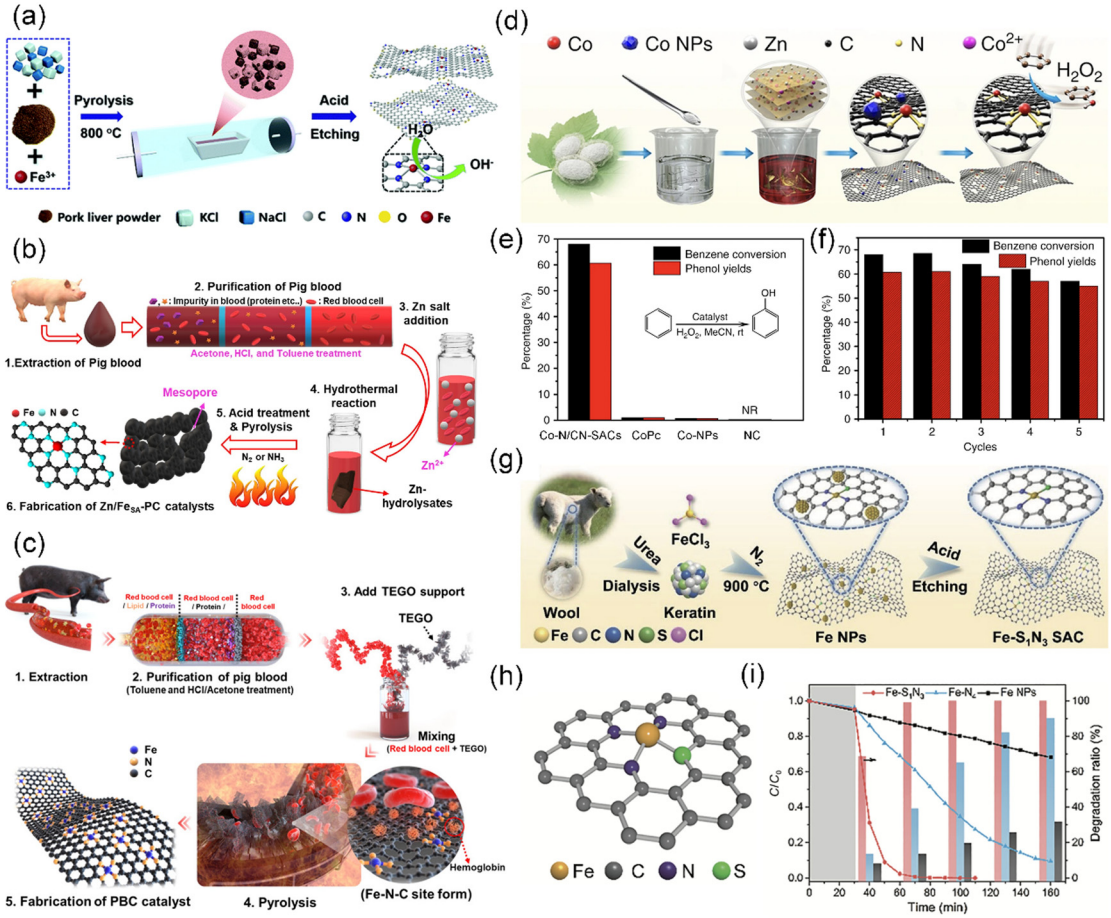

Fig. 11 (a) Schematic showing the preparation of Fe–N/CS-SACs. Reproduced with permission from ref. 62 (Copyright 2021, The Royal Society of Chemistry). Schematic illustration of the preparation of (b) Zn-incorporated Fe single-atom porous carbon (designated Zn/Fe_{SA}-PC) catalyst and (c) pig blood-derived carbon (PBC) catalyst. (b) Reproduced with permission from ref. 190 (Copyright 2021, The Royal Society of Chemistry). (c) Reproduced with permission from ref. 191 (Copyright 2021, the American Chemical Society). (d) Synthetic process of Co–N/CN-SACs. (e) Comparison of benzene oxidation catalyzed by Co–N/CN-SACs, cobalt phthalocyanine (CoPc), Co nanoparticles/N-doped carbon (Co-NPs), and N-doped carbon (NC). (f) Recycling performance of Co–N/CN-SACs. (d)–(f) Reproduced with permission from ref. 192 (Copyright 2018, Springer Nature). (g) Schematic illustration of synthetic procedure for Fe–S_1N_3 SAC. (h) Atomic structure three-dimensional model of Fe–S_1N_3. (i) Removal efficiency of methylene blue (MB), RhB, and phenol using Fe–S_1N_3, Fe–N_4 (single Fe atom supported on N-doped carbon prepared from natural silk fibroin carrier without S), and Fe NPs (Fe nanoparticles/N-doped carbon prepared from natural silk fibroin carrier). (g)–(i) Reproduced with permission from ref. 193 (Copyright 2023, Springer Nature).

only natural cationic amino polysaccharide, comprised of repeating units of *N*-acetyl-D-glucosamine and D-glucosamine, which are linked by β-(1–4) glycosidic linkages.[174,201] Importantly, chitosan possesses a high N content (approximately 7 wt%) due to its N-containing functional groups such as amines and acetamides, making it a suitable precursor for the synthesis of N-doped carbon materials.[202] Additionally, given a large amount of –OH and –NH_2 groups on the molecular chain, chitosan can coordinate with transition metals or rare earth metal ions to form chitosan metal complexes, which are ideal precursors for the preparation of SACs.[39,203–206]

It is imperative to explore innovative approaches to harness the chitosan resource for sustainable development due to the millions of tons of seafood waste disposed of annually. Zhu *et al.* designed a scalable approach to fabricate gram-scale Co-based SACs anchored on N-doped porous carbon nanobelt (Co–N/PCN-SACs) *via* the carbonization of chitosan for the selective oxidation of aromatic alkanes in water at room temperature (Fig. 12a).[203] By using $ZnCl_2$ and $CoCl_2$ salts as effective activation–graphitization agents, a porous belt-like nanostructure (Fig. 12b) was achieved, as shown by the ultra-high specific surface area (2513 $m^2\ g^{-1}$), large pore volume (2.2 $cm^3\ g^{-1}$), and high graphitization degree. In the oxidation of ethylbenzene, the Co–N/PCN-SACs showed a remarkable catalytic efficiency with 98% conversion and 99% acetophenone selectivity (Fig. 12c and d, respectively). By using NH_4Cl salt as a foaming agent, Wang *et al.* controllably synthesized scalable Co-based SACs anchored on an N-doped 3D ultrathin porous carbon sheet derived from chitosan with a super-high specific surface area of 1977.9 $m^2\ g^{-1}$.[39] Liu *et al.* reported a highly dispersed Ru catalyst supported by N-doped carbon derived from chitosan (RuN/ZnO/C) with an extremely low loading, which showed an outstanding performance in the reductive catalytic fractionation of lignocellulose (Fig. 12e).[204]

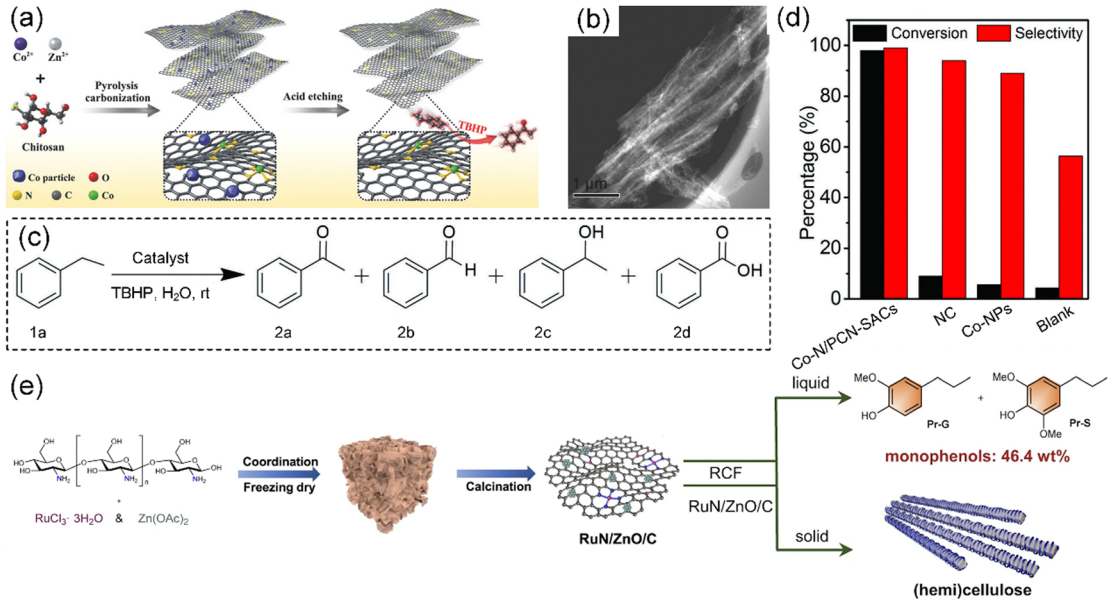

Fig. 12 (a) Preparation of Co–N/PCN-SACs. (b) Typical STEM image of Co–N/PCN-SACs. (c) Reaction model of selective oxidation of ethylbenzene. (d) Catalytic activity for ethylbenzene oxidation by Co–N/PCN-SACs, NC (N-doped carbons), Co-NPs (Co nanoparticles), and blank condition. (a)–(d) Reproduced with permission from ref. 203 (Copyright 2018, Wiley). (e) Illustration of the fabrication process for RuN/ZnO/C catalyst and reductive catalytic fractionation of lignocellulose for RuN/ZnO/C catalyst. Reproduced with permission from ref. 204 (Copyright 2022, Springer Nature).

This Ru catalyst afforded maximum yields of phenolic monomers (46.4 wt%) from lignin, while the cellulose and hemicellulose components were preserved. In this method, Zn species were introduced in the Ru catalyst as Lewis acid centers to promote the hydrogen hydrolysis of the β-O-4 unit.

5.2.2 Gelatin. Gelatin is an animal derivative that is generally produced from the partial hydrolysis of collagen extracted from the skins and bones of animals, *e.g.*, porcine (pork), bovine (beef or cattle), and fish.[207,208] As a mixture of proteins and peptides, gelatin is made up of 18 different types of intricate amino acids, which have an average N content of 16%. It predominantly consists of approximately 57% glycine, proline, and hydroxyproline, while the remaining components are other amino acid families, including glutamic acid, alanine, arginine, histidine, and aspartic acid.[209] Histidine molecules containing amine functional groups, carboxyl groups, and imidazole groups, which can be strongly coordinated with Fe^{3+} ions, have been used to prepare Fe-based SACs on N-doped carbon nanospheres (Fe–N/CN-SACs) (Fig. 13a).[63] Due to their atomically dispersed Fe–N_4 sites and unique spherical hollow architecture, the as-synthesized Fe–N/CN-SACs displayed an outstanding performance in the ORR under alkaline conditions (Fig. 13b and c). Gelatin has been widely explored by researchers because it is a naturally abundant and sustainable resource with high solubility in polar solvents and high N content. Wang *et al.* introduced a novel strategy to simultaneously produce nonprecious Fe–N–C catalysts and Fe_3O_4/N-doped carbon hybrids by utilizing the coordinating capabilities of carboxyl and amide groups in gelatin with metal ions (Fig. 13d).[207] The decomposition of ammonium nitrate during the carbonization process generated a large amount of micropores and mesopores in the Fe–N–C catalyst, with a high surface area of 1215.4 m^2 g^{-1} (Fig. 13e).

In addition, carbon aerogels derived from biobased hydrogels, which are 3D materials with rich porosity and nanowrinkles, have been extensively investigated for the preparation of SACs. The spatial confinement of the micropores and nanowrinkles in carbon aerogels not only facilitates the incorporation of isolated metal atoms but also boosts the intrinsic activity of the atomic sites.[80,210,211] He *et al.* prepared RuN_x-based SACs coupled with Ru nanoclusters that were embedded in carbon aerogels by using a gelatin-zinc hydrogel (G_{Si}/Ru-PM) as the structural template and SiO_2 nanoparticles as the porogen, while using a ruthenium-phenanthroline (Ru-PM) complex as the metal and N sources. The RuN_x-based SACs showed a remarkable performance in the hydrogen evolution reaction (HER) in a broad range of solution pH.[211] Subsequently, Fe-based SACs with adjacent Fe nanoclusters supported by N-doped carbon aerogels (NCA/Fe_{SA+NC}) were fabricated through the facile two-step carbonization of a gelatin hydrogel containing an Fe-phenanthroline (Fe-PM) complex, while nano-SiO_2 was used as the template.[210] The HAADF-STEM analysis showed that the NCA/Fe_{SA+NC} composites contained both metal nanoclusters (under 10 nm in diameter) and individual metal atoms (Fig. 13g and h). The Fe atomic centers displayed a high 3d electron density and reduced magnetic moment because of the adjacent metal nanoclusters, leading to favorable impacts on the electrocatalytic activity and oxidative stability in the ORR and OER. Remarkably, the Zn–air battery assembled using the NCA/Fe_{SA+NC} catalysts delivered a freeze-tolerant performance (Fig. 13i).

5.3 Small-molecule compounds

Dopamine (DA) is a type of catecholamine consisting of a 3,4-dihydroxy-substituted phenyl ring, which is widely found in animals, where it is known as a neurotransmitter.[212] Marine mussels have a remarkable ability to adhere to nearly all

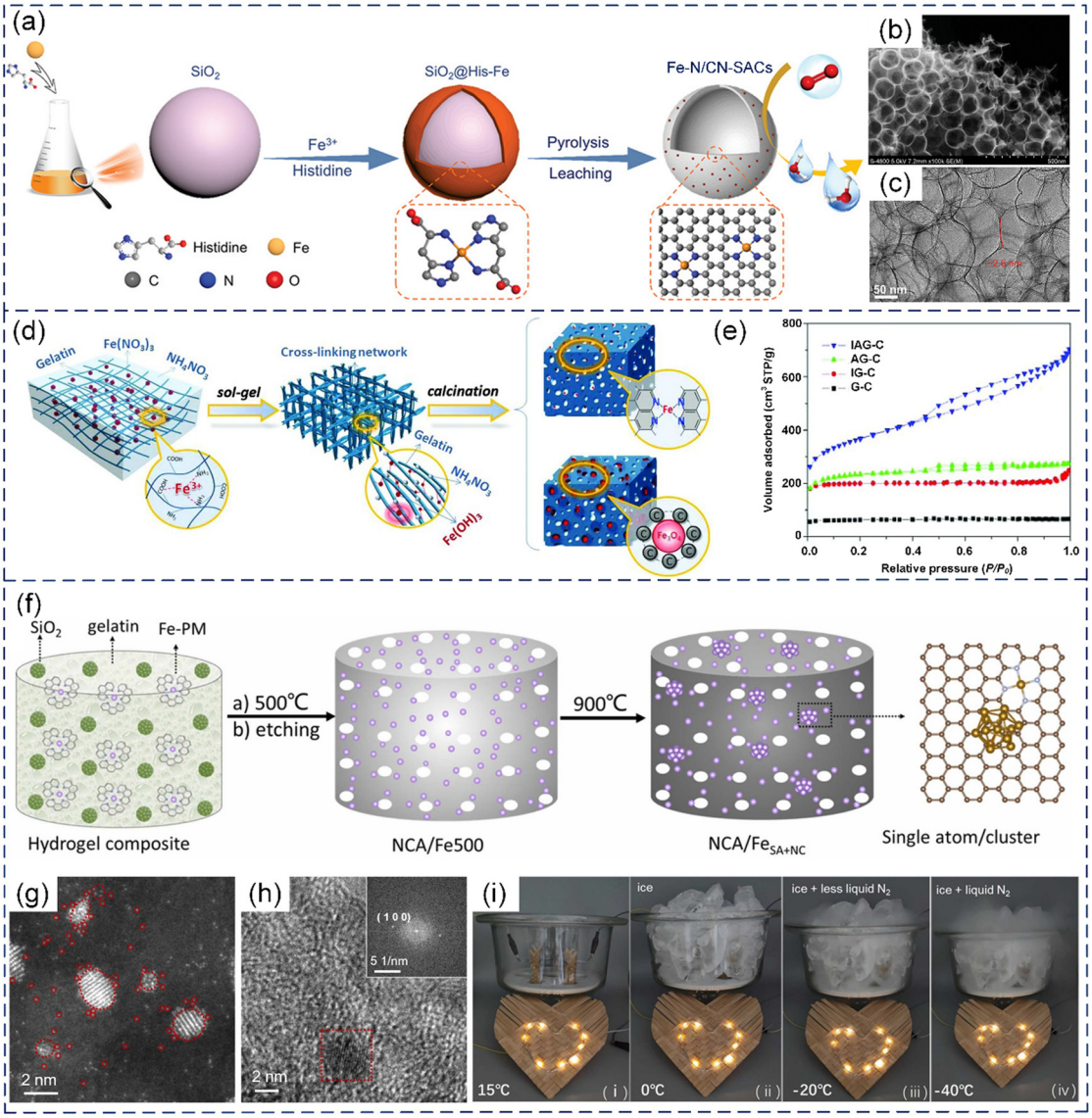

Fig. 13 (a) Schematic illustration of the synthetic process, (b) SEM image, and (c) TEM image of Fe–N/CN-SACs. (a)–(c) Reproduced with permission from ref. 63 (Copyright 2018, Wiley). (d) Illustration of the procedure for the preparation of IAG-C catalysts (*i.e.*, Fe–N–C catalyst: $Fe(NO_3)_3$, NH_4NO_3, and gelatin as precursor components) and Fe_3O_4@AGC (Fe_3O_4/N-doped carbon hybrid) electrode materials. (e) Nitrogen adsorption–desorption curves of four samples prepared with different precursors (AG-C: ammonium nitrate and gelatin; IG-C: iron nitrate and gelatin; and G-C: pure gelatin). (d) and (e) Reproduced with permission from ref. 207 (Copyright 2015, AAAS). (f) Schematic illustration of the preparation of NCA/Fe_{SA+NC}. (g) HAADF-STEM images of NCA/Fe_{SA+NC}. (h) High-resolution transmission electron microscopy (HRTEM) image of a typical metal cluster in NCA/Fe_{SA+NC}. The inset shows the Fourier transform of the red region. (i) Photographs of an LED pattern powered by two Zn//NCA/Fe_{SA+NC} batteries in series at different temperatures. (f)–(i) Reproduced with permission from ref. 210 (Copyright 2023, ScienceDirect).

inorganic and organic surfaces due to their adhesive proteins. DA, inspired by the catecholamines present in the adhesive proteins of marine mussels, was utilized for the synthesis of polydopamine (PDA) through a self-polymerization process under alkaline conditions, which could be coated on nearly all natural or synthetic substrates, *e.g.*, metals, oxides, polymers, ceramics, bacteria, and cells (Fig. 14a and b).[174,213] In addition, DA is also a type of polyphenol that consists of two hydroxyl groups, one aromatic ring and one ethylamine, possessing the ability to coordinate with metal ions, especially with transition metal ions (Fig. 14c).[214]

Inspired by the universal coating capability of PDA, Zhang *et al.* synthesized SACs dispersed on hollow N-doped carbon materials (Fe–N/CS-SACs) by carbonizing PDA-coated α-FeOOH nanorods (α-FeOOH@PDA) and subsequent acid leaching (Fig. 14d and e).[78] By changing the metal precursors or polymers, N-doped carbon materials anchored by different metal single atoms (M–N/CS-SACs, M = Fe, Co, Ni, Mn, FeCo, FeNi, *etc.*) were successfully synthesized. Remarkably, the resultant Fe–N/CS-SACs exhibited a high conversion of 45% and high selectivity of 94% in the direct hydroxylation of benzene to produce phenol (Fig. 14f). SiO_2 is also frequently used as a

template for PDA coatings in the fabrication of CS-SACs.[215,218] For instance, Zhang *et al.* obtained Ni-based SACs anchored on N-doped hollow carbon spheres (Ni–N/CS-SACs) through the carbonization of the formed core–shell SiO_2@polydopamine/Ni(acac)$_2$ structure by controlling the Ni loading and carbonization temperature, which were an excellent catalyst for electrochemical oxidation of NO (Fig. 14g).[215] The EDX elemental analysis showed that the C, N, and Ni elements in the Ni–N/CS-

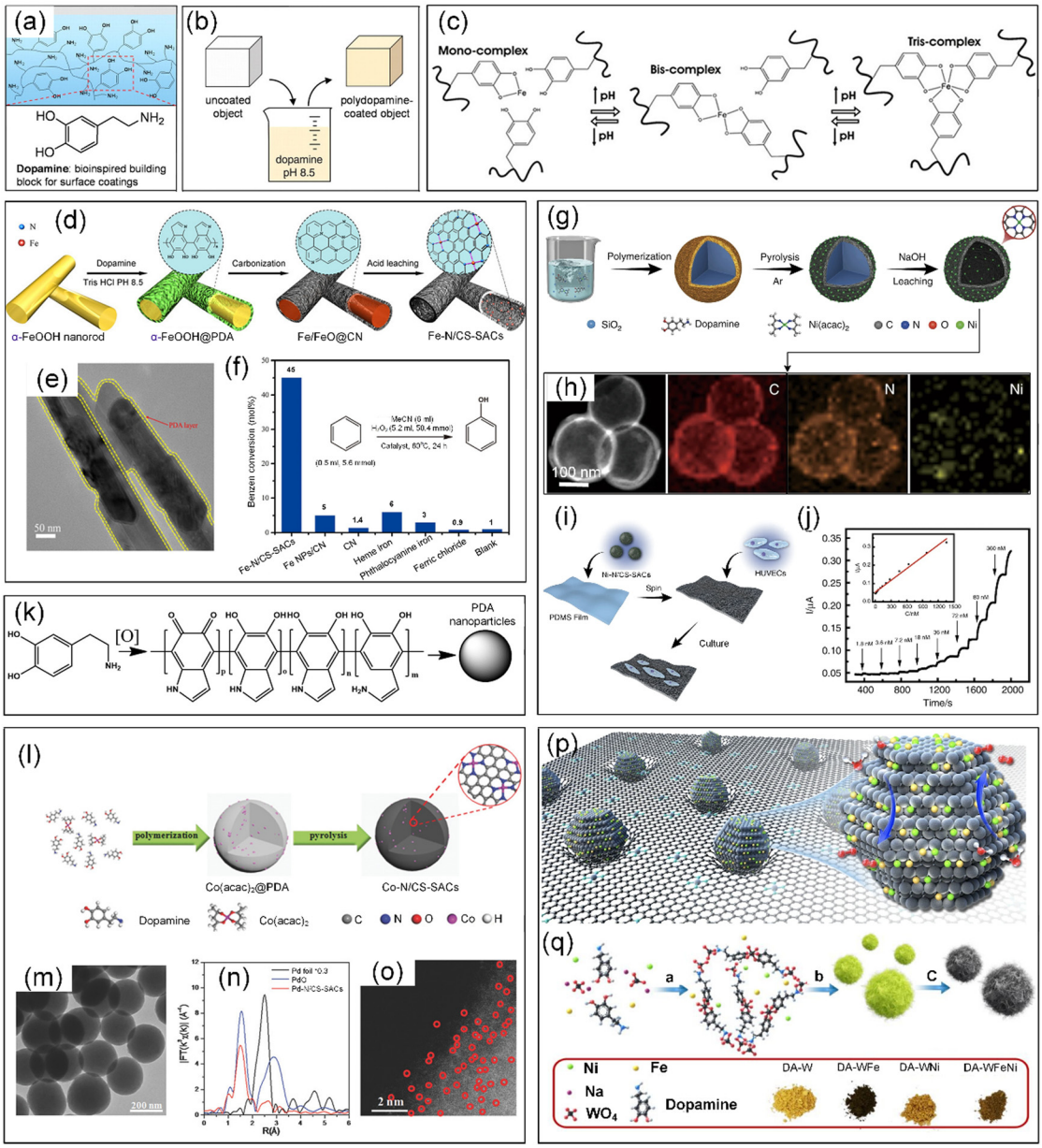

Fig. 14 (a) Marine mussel-inspired DA building block for surface coating. (b) Schematic illustration of PDA thin film deposition by dip-coating an object in an alkaline DA solution. (a) and (b) Reproduced with permission from ref. 213 (Copyright 2007, AAAS). (c) Cross-linking reaction between catechol groups in DA and Fe^{3+} ions. Reproduced with permission from ref. 214 (Copyright 2014, the American Chemical Society). (d) Preparation of Fe–N/CS-SACs. (e) TEM image of α-FeOOH@PDA. (f) Benzene conversion was catalyzed by different materials. (d–f) Reproduced with permission from ref. 78 (Copyright 2017, the American Chemical Society). (g) Synthesis and (h) HAADF-STEM image and corresponding EDX element mapping of Ni–N/CS-SACs. (i) Schematic illustration of the fabrication of Ni–N/CS-SAC-based stretchable sensor for NO sensing and culturing HUVECs: PDMS film (polydimethylsiloxane) and HUVECs (human umbilical vein endothelial cells). (j) Amperometric response of the Ni–N/CS-SAC-based stretchable sensor (0.5 cm^2) to the successive addition of NO at +0.80 V. Inset, calibration curve. (g)–(j) Reproduced with permission from ref. 215 (Copyright 2020, Springer Nature). (k) Scheme of the synthesis of PDA nanoparticles by oxidation of DA. Reproduced with permission from ref. 216 (Copyright 2018, the American Chemical Society). (l) Synthesis of Co–N/CS-SAC nanospheres. (m) TEM images of Co–N/CS-SAC nanospheres. (n) Pd K-edge of Pd–N/CS-SAC nanospheres, PdO, and Pd foil. (o) AC HAADF-STEM image of Pd–N/CS-SAC nanospheres. (l)–(o) Reproduced with permission from ref. 217 (Copyright 2018, Wiley). (p) Schematic illustration of WC_x–FeNi catalyst. (q) Schematic illustration of the synthetic procedures. (p) and (q) Reproduced with permission from ref. 38 (Copyright 2021, Springer Nature).

SACs were homogeneously distributed over the entire architecture (Fig. 14h). Significantly, the electrocatalyst based on Ni–N/CS-SACs enabled the real-time detection of a trace amount of NO released from endothelial cells in response to drug and stretch stimulation (Fig. 14i and j).

In addition, DA can also self-assemble into PDA nanoparticles with a size ranging from several nanometres to hundreds of nanometres in aqueous alkaline solutions or after oxidation treatment, which was employed to manufacture CS-SACs (Fig. 14k).[82,174,216,219] Han *et al.* prepared metal SACs supported by porous N-doped carbon nanospheres with a high surface area of $\sim$380 m^2 g^{-1} through a facile polymer encapsulation strategy *via* simply mixing the corresponding metal acetylacetonate complexes with DA monomers (Fig. 14l and m).[217] This approach can be used for the preparation of SACs employing both precious and non-precious metals (M-SACs, where M includes Co, Ni, Cu, Mn, and Pd) (Fig. 14n and o). Considering that the strong coordination between heteroatoms and catalytic metal sites affects the electronic environment (d-band center) of the metal atoms, and consequently the catalytic activity, Li *et al.* introduced a technique to construct atomic or bi-atomic metals (Fe, Ni, and FeNi) on transition metal carbides (TMCs) to yield highly efficient single-atom OER catalysts without heteroatom coordination (Fig. 14p).[38] Specifically, WC_x–Fe, WC_x–Ni, and WC_x–FeNi catalysts were obtained by the carbonization of a DA tungstate complex, which was formed by DA molecules with Fe, Ni, or FeNi ions and tungstate ions in a precipitation reaction because of the unique structure of tungsten carbides (Fig. 14q).

Animal-derived biomass possesses more complex compositions compared with plant-based precursors. N atoms are the most similar characteristics of the supports prepared from animal-based precursors, where chitin and proteins are the representative ones. The unpaired electrons in N atoms improve the thermal stability of CS-SACs and enhance the binding between the supports and metal atoms. The intrinsic presence of N avoids the utilization of an external N-source during carbonization, which is ideal at the industrial scale. Animal biomass derived from shells contains abundant *N*-acetyl groups, resulting in high thermal stability, but also requires deacetylation procedures during pre-carbonization to gain better control of the support structures for CS-SACs. Generally, hybridization is employed animal-based biomass to for structure inheritance after carbonization as precursors from plants. The hard inorganic templates (*e.g.*, SiO_2) guide the structure formation in the precursors, further leaving channels or patterns in the resulting supports after carbonization.

6. CS-SACs from microbial biomass

Microbial biomass, especially algae/seaweed-based species, is a promising precursor for the synthesis of SACs due to its high content of heteroatoms and metal ions.[52–54,92] In this section, several microbial biomass precursors for the synthesis of CS-SACs are introduced, including eukaryotic organisms (macrofungi, macroalgae, and microalgae) as well as prokaryotic organisms (microalgae and bacteria).

6.1 Eukaryotic organisms

6.1.1 Macrofungi. *Auricularia auricula-judae* (*AAJ*), belonging to the genus *Auricularia* of *Basidiomycetes* in the family *Auriculariaceae*, is a special type of mushroom, and also the third most cultivated edible fungus in the world.[220] Furthermore, it is also widely used as traditional medicinal ingredients, fermented foods, noodles, and antibiotic oxidants.[221] Importantly, *AAJ* has abundant N and Fe elements in its enzymes and ferritin. Wang *et al.* reported a strategy to synthesize Fe-SACs supported by N-doped carbon (Fe–N/CS-SACs) using Fe sources from the catalyst precursor of *AAJ* (Fig. 15a).[55] The Fe–N/CS-SACs exhibited excellent ORR activities, stability, and methanol tolerance, which could be used in energy conversion systems (Fig. 15b and c).

6.1.2 Macroalgae. *Porphyra* is a cold-water seaweed that grows in shallow and cold seawater, which is rich in alginate, *e.g.*, alginic acid, sodium alginate, ammonium alginates, and calcium alginate.[152] Sodium alginate is composed of α-L-guluronic and β-D-mannuronic acid units with numerous hydrophilic groups, facilitating the formation of a hydrogel with metal ions through the coordination reaction in an aqueous solution.[224,225] Moreover, sodium alginate can effectively immobilize target metal ions through the formation of a special ''egg-box'' structured metal–organic polymer supramolecule, making it an excellent precursor for the synthesis of CS-SACs.[225,226] Zhang *et al.* introduced a universal approach for fabricating M-SACs (M = Co, Ni, and Cu) on reduced graphene oxide by utilizing earth-abundant sodium alginate as the precursor, while using melamine as the N source, and Zn salt as the sacrificial template.[226] In the formation of Co-SACs, the evaporation of Zn in the carbonization process serves dual purposes, *i.e.*, it not only creates channels for the entry of acid but also provides defects for anchoring atomic Co species. Similarly, Fe-SACs were also successfully designed by the carbonization of an aerogel consisting of sodium alginate and Fe ions.[225]

Porphyra has inherent heteroatom and abundant amino acids, which is a promising precursor for N-doped carbon[227] and an outstanding precursor material for electrocatalyst preparation.[228] Zhang *et al.* reported a strategy to prepare Fe–N_x moiety-modified N-doped hierarchically porous carbons derived from porphyra.[227] The resultant electrocatalysts showed an excellent ORR performance. Zhang *et al.* also used *Porphyra* to synthesize Fe-based SACs supported by N-doped hierarchically porous carbon (Fe-SACs/NHPC) for the ORR, which exhibited outstanding catalytic activity and catalyst stability (Fig. 15d).[222] Cao *et al.* designed a method to synthesize Fe/Pt single-atom electrocatalysts anchored on N-doped carbon derived from *Porphyra* biomass, which is potentially used for applications of hydrogen economy.[229]

Enteromorpha, a kind of green algae in the family *Ulvaceae*, has abundant nitrogenous compounds, *e.g.*, polysaccharides, vitamins, proteins, and Fe elements.[52,230] The high amounts of N and Fe in *Enteromorpha* can be incorporated in carbonaceous materials after *in situ* carbonization, converting *Enteromorpha*

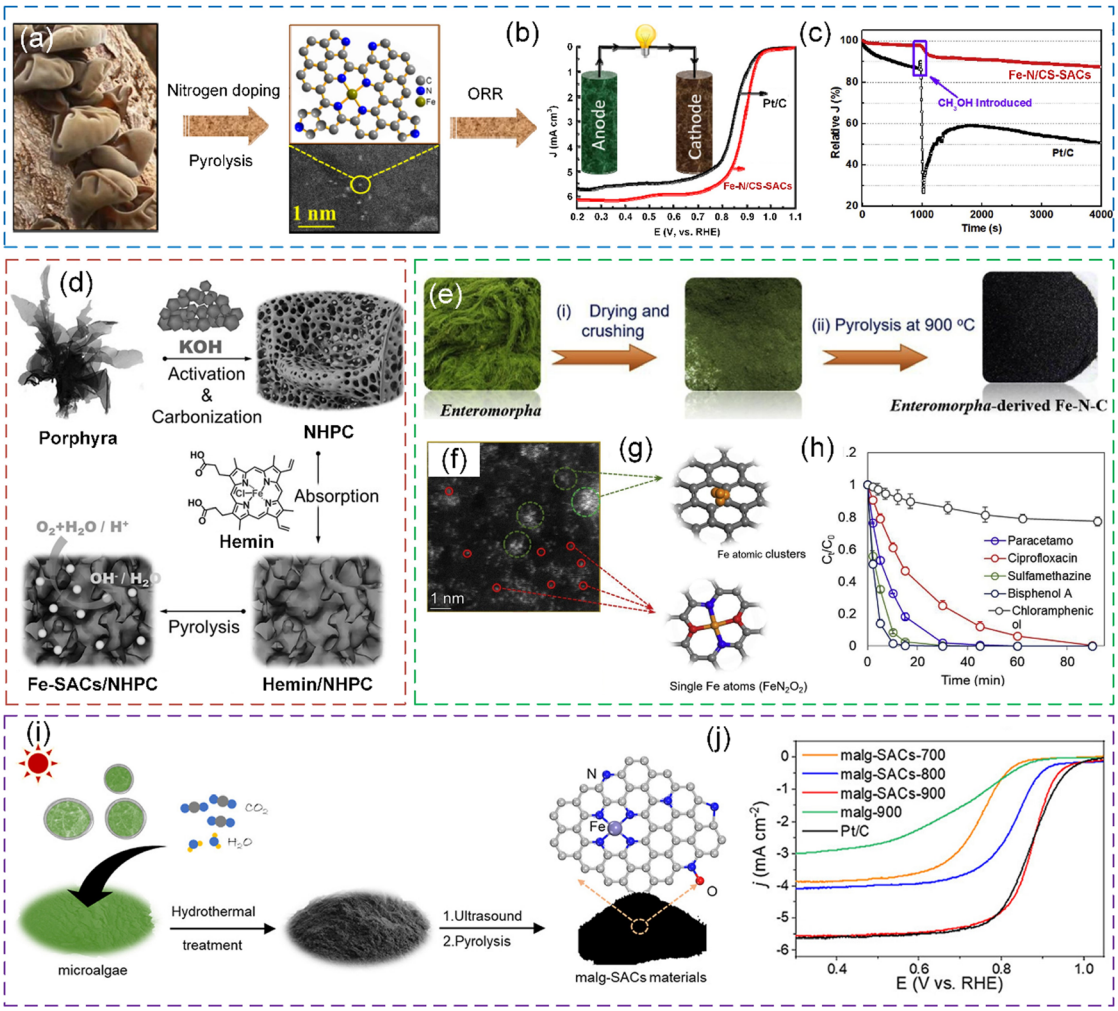

Fig. 15 (a) Synthesis process of Fe–N/CS-SACs using *AAJ* as the precursor. (b) ORR polarization curves of Fe–N/CS-SACs and Pt/C. (c) Methanol resistance of Fe–N/CS-SACs and Pt/C in 0.1 M KOH saturated with O_2 at 0.7 V. The purple rectangle shows the addition of 10% (v/v) methanol to the electrochemical cell. (a)–(c) Reproduced with permission from ref. 55 (Copyright 2023, the American Chemical Society). (d) Schematic illustration of the preparation process of Fe-SAC/NHPC electrocatalyst. Reproduced with permission from ref. 222 (Copyright 2017, Wiley). (e) Fabrication scheme and (f) HAADF-STEM image of *Enteromorpha*-derived Fe–N–C. (g) Simulated structures of Fe atomic clusters and single-atom Fe sites. (h) Degradation of different pollutants in *Enteromorpha*-derived Fe–N–C/PMS system. (e)–(h) Reproduced with permission from ref. 53 (Copyright 2021, ScienceDirect). (i) Schematic illustration of the procedure for the synthesis of malg-SACs-X from microalgae biomass. (j) Polarization curves for the malg-SACs products and Pt/C catalysts. (i) and (j) Reproduced with permission from ref. 223 (Copyright 2023, ScienceDirect).

from a seawater pollutant into a carbon catalyst for the degradation of organics.[231] Peng *et al.* reported that after the direct carbonization of *Enteromorpha*, Fe clusters and dispersed Fe–N_x sites derived from the intrinsic Fe in *Enteromorpha* were observed (Fig. 15e–g).[53] Chen *et al.* designed a process to fabricate an N and Fe co-doped carbonaceous material (Fe–N@C) *via* the thermal treatment of *Enteromorpha*, and the as-prepared carbon-based Fe catalysts exhibited high stability, which allowed it to be used for environmental remediation.[52] The PMS activation of *Enteromorpha*-derived carbocatalyst was investigated in the studies by Peng *et al.* and Chen *et al.* (Fig. 15h).

6.1.3 Microalgae. *Chlorella*, a spherical single-celled alga with a diameter in the range of 3 to 8 μm, is one of the most cultivated eukaryotic green microalgae and is widely used in pharmaceuticals, beauty care products, health food, and feed supplements.[232] *Chlorella* is also a valuable precursor for SACs due to its large specific surface area, inherent N elements, and heavy metals absorbed by its rich amino groups. Wu *et al.* demonstrated a strategy to prepare porous SACs with well-dispersed Co–N_4 sites (Co–N/CS-SACs) by using *Chlorella* as the precursor and NaCl/KCl eutectic system-assisted carbonization.[35] The resulting Co–N/CS-SACs exhibited good catalytic activity comparable to that of Pt catalysts, which could be potentially used as an ORR catalyst in an alkaline medium.

Scenedesmus obliquus NIES-2280, a typical freshwater chlorophyte with a rapid growth rate, possesses a robust uptake capacity of CO_2 and nutrient elements (N and P).[233] Particularly, the membrane-bound cells have abundant metal-containing biomolecules that could be used as metal sources.[223,234] Ma *et al.* reported a method to prepare Fe-SACs for ORR through the direct conversion of *Scenedesmus obliquus NIES-2280* using endogenous metals and introducing an exogenous N source

from g-C_3N_4 (Fig. 15i and j).[223] In the high-temperature carbonization, g-C_3N_4 plays a critical role in the formation of hierarchical porous structures and doping N heteroatom.

6.2 Prokaryotic organisms

6.2.1 Microalgae. *Spirulina* is a widespread aquatic alga endowed with high protein content (up to 60%) and abundant hydrogenase.[54,235] *Spirulina* is a promising substrate for SACs when converted to biochar, while the N source can be incorporated from its protein components. *Spirulina*, if converted to biochar, can be a cheap alternative to graphene and carbon nanotubes for the preparation of SACs due to its abundant sources.[236] Ho *et al.* reported a strategy to prepare N-doped graphitic biochar through the conversion of the non-disposable *Spirulina* waste after C-phycocyanin extraction. It showed that the salt-containing *Spirulina* can be converted into a green carbon catalyst for purifying microcontaminants and disinfecting in wastewater treatment.[92] Mn-based SACs (Mn-SACs) were prepared by embedding single-atom Mn in *Spirulina*-based biochar through high-energy ball milling and calcination of Mn-doped polymeric carbon nitride and biochar.[236] The resulting Mn-SACs showed an excellent catalytic performance in removing enrofloxacin from water. Particularly, hydrogenase with an S-coordinated Fe atom as the center in *Spirulin*a makes *Spirulina* a potential N,S co-doped Fe source.[235] Lei *et al.* reported a strategy to prepare Fe-SACs coupled with ultra-small Fe_2O_3 nanoclusters that were embedded in N,S-co-doped porous carbons *via* the *in situ* conversion of *Spirulina*.[54] The resulting metal electrocatalysts showed an outstanding ORR performance, surpassing the most advanced non-noble metal catalysts.

6.2.2 Bacteria. The electroactive bacterium GS has a large network of multiheme-containing outer-membrane c-Cyts,[237] which endows them with a unique respiratory pathway and extracellular electron transfer (EET) pathway, and the EET capability of GS allows them selected as a targeted bacterium for practical biotechnological applications and preparation of electrocatalysts.[238] Pedireddy *et al.* designed an approach to synthesize M-SACs (M = Fe, Ir, Pt, Ru, Cu, or Pd) at room temperature by using the EET capability of GS, which could be used for various electrocatalytic reactions.[88] Besides harnessing the properties of bacterial organisms, nanocellulose produced by bacteria, which is known as bacterial cellulose, can adsorb metal ions due to its abundant oxygen groups, which has been also considered a viable candidate for producing CS-SACs.[152,239] High-density, atomically dispersed, bimetallic Fe–Co single-atom electrocatalysts with a desired Fe/Co ratio and loading were successfully fabricated by utilizing bacterial cellulose to anchor Fe and Co.[239] Ammonia plays a key role in the production of fertilizers and various valuable chemicals in different industries. In the electrocatalytic NRR, the as-designed catalysts achieved a remarkable ammonia yield rate of 579.2 ± 27.8 μg h^{-1} $mg_{cat.}{}^{-1}$ and exceptional faradaic efficiency of 79.0% ± 3.8%.

Microbial biomass is an important non-negligible source for CS-SACs, typically algae, due to their rapid growth, good environmental tolerance, and solar energy storage. The rich nutrient contents enable the introduction of diverse heteroatoms and structures in the derived carbonaceous supports. These precursors are a promising sustainable energy feedstock and the alternatives for fossil fuels as the consumption of greenhouse gas during their growth. The main disadvantages also come from the high nutrients due the production of a wide product distribution. Extraction is preferred to remove the lipids from bio-oil products in the context of biorefinery. The disadvantages of microbes are the diverse and versatile characteristics and qualities of the generated CS-SACs from different species. Accordingly, pre-treatment such as extraction is recommended prior to carbonization.

7. Conclusions and perspective

Biomass found in nature offers not only captivating bio-inspired strategies for materials science but also a versatile toolbox of natural building blocks for the creation and development of innovative functional materials. The development of SACs using biomass sources as fundamental building blocks has accelerated the progress in the field of catalysis, opening up a new avenue for converting biomass into value-added products. Biomass-derived carbon materials provide an excellent support for SACs, enabling the *in situ* incorporation of metal atoms in the carbon matrix, while the inherent O, N, and S elements in many biomasses even waste biomass can serve as for anchoring the metal atoms. Moreover, naturally derived biomass, such as chitosan, starch, gelatin, cellulose, lignin, and polyphenol, can also be used as alternative ligands or an N-rich source for *in situ* doping and complexation during the synthesis of CS-SACs. This review highlighted the recent advancements related to the synthesis strategies, different types of biomass precursors, geometric and electronic properties and catalysis applications of various CS-SACs derived from biomass based on the considerable number of relevant published articles at the current stage. The various biomasses employed for the preparation of CS-SACs are summarized in Table 2. Particularly, these biomass-derived CS-SACs have wide potential in different application fields, including electrochemistry, fuel cells, water treatment, biosensors, and fine chemicals, which can realize the high-value utilization of biomass sources and are conducive to sustainable development.

The remarkable activity of SACs is predominantly attributed to the abundant presence of active sites. Despite the numerous natural biomasses that have recently been used to prepare CS-SACs, the synthesis of CS-SACs with a high metal loading (>10 wt%) remains an unsolved challenge. Generally, increasing the metal loading can further enhance the catalytic performance. Nevertheless, the high metal loading and stability of single atomic dispersions are usually mutually exclusive, which is an inherent dilemma in classical material design for SACs. The individual metal atoms easily undergo migration, agglomeration, and sintering during preparation and catalytic reactions due to their high surface energy, affecting the stability of SACs and reducing their overall catalytic activity. A high metal loading and long-term stability are the aim to realize ideal SACs.

Table 2 Summary of various biomasses employed for the preparation of CS-SACs

Biomass	Metal source	Heteroatom source	SACs	Loading (wt%)	Configuration	Catalytic application	Ref.
Natural wood	$FeCl_3·6H_2O$	Ar-NH_3	SAC-FeN-WPC	0.8	Fe–N_4	ORR/OER/Zn–air batteries	112
	$Ni(NO_3)_2·6H_2O$	Urea	Ni SAs-NCW	0.13	Ni–N_4	CO_2 reduction reaction	113
P. americana	Accumulating Mn from $MnCl_2·4H_2O$	Urea	Mn SAC	4.44, 1.13	Mn–N_4	PMS-driven organics degradation	56, 123
M. aquaticum	K_2FeO_4	—	ISA-Fe/MC	2.4	—	PMS-driven phenol degradation	127
Waste ferns	Fern contaminated by Fe mines	$NH_3·H_2O$	Fe SAC	0.04	Fe–N_4	PMS-driven quinolone antibiotic degradation	128
Corn silk	$Fe(NO_3)_3·9H_2O$	Melamine	Fe SA/NCZ	4.30	Fe–N_4	ORR/OER/Zn–air batteries	135
Coffee grounds	$CoCl_2·6H_2O$	Intrinsic N, S	Co SAC	1.13	Co–N_3S_1	PMS-driven organics degradation	136
Waste paper	TCPP-Co	Polyethyleneimine	Co–N_3/WPAC	—	Co–N_3	Persulfate (PS)-driven sulfisoxazole degradation	137
Starch	Metal chlorides	Dicyandiamide, boric acid	ISAS M/NBPC (M = Co, Fe, or Ni)	1.5–2.1	M–N_3B_1	Various catalytic reactions	40
Cellulose	$Cu(NO_3)_2·3H_2O$	1,10-Phenanthroline monohydrate (PM)	Cu-SACs	4.08	Cu–N_4	PMS-driven oxytetracycline degradation	164
	$Co(CH_3COO)_2·4H_2O$	NH_4Cl	Co SAs/NCNA	0.11	Co–N_4	ORR/Zn–air batteries	157
	Metal nitrates	Inherent C and O	M-SACs (M = Fe, Co, Ni, Cu, and Zn)	0.29–1.15	M–O_3C	Tetracycline photocatalytic removal	158
Lignin	Metal nitrates	Dicyandiamide	M SAs-N@C (M = Fe, Co, Ni, Cu)	1.47–5.44	M–N_3C	An integrated biorefinery	59
	$Zn(NO_3)_2$	Lignin alkali	ZnN_4-SAC	0.67	Zn–N_4	Oxidative cleavage of C–N bonds	173
Polyphenol	Metal nitrates	NH_3	M-SAC (M = Co, Fe, Mn, Co–Mn, Fe–Mn)	2.09–5.50	M–N_4	Oxygen reduction and photocatalytic activity	37
	$Co(OAc)_2·4H_2O$	HCCP	PAST-Co-1000	10.12	Co–N_2P_2	ORR	189
Pig liver	$Fe(NO_3)_3$	N in protein	Fe–N/C-SAC	2.60	Fe–N_4	ORR	62
Pig blood	Fe-porphyrin	N in hemoglobin	Fe–N–C	—	Fe–N_x	ORR	196
	—	—	Fe SACs	0.5–1.3, 1.3–1.9	Fe–N_4	Zn–air batteries/anion exchange membrane fuel cells	190, 191
Silk fibers	Metal nitrates	N in silk fibroin	M-ISA/CNS (M = Fe, Co, Ni)	0.6	Co–N_4	Hydroxylation of benzene to phenol	192
	$FeCl_3·6H_2O$	—	Fe–N_x–C	0.12	Fe–N_4	ORR	198
Wool	$FeCl_3·6H_2O$	N and S in protein keratin	Fe–S_1N_3 SACs	1.16	Fe–S_1N_3	Fenton-like catalysis	193
Chitosan	$CoCl_2·6H_2O$	Inherent N	Co-ISA/CNB	0.1	Co–N_4	Oxidation of ethylbenzene	203
	$Co(Ac)_2·4H_2O$	—	Co SANC	1.27	Co–N_4	ORR/metal–air batteries	39
	$RuCl_3·3H_2O$	—	RuN/ZnO/C	0.12	Ru–N_4	Reductive catalytic fractionation of lignocellulose	204
	$Na_2MoO_4·2H_2O$	—	Mo-SAs	1.32	Mo–N_1C_2	HER	206
Histidine	$Fe(NO_3)_3·9H_2O$	Inherent N	Fe–N–C HNSs	1.4	Fe–N_4	ORR	63
Gelatin	$Fe(NO_3)_3·9H_2O$	Inherent N	Fe–N–C	0.14	Fe–N_4	ORR	207
	$FeCl_2·4H_2O$	Inherent N	NCA_{C-Zn}/Fe	0.72	Fe–N_4	ORR/OER/Zn–air batteries	80
	$RuCl_3$	PM	NCAG/Ru	0.47	RuN_xC_{4-}–O	HER	211
	$FeCl_2·4H_2O$	PM	NCA/Fe_{SA+NC}	1.73	Fe–N_4	ORR/Zn–air batteries	210
Dopamine	Metal(hydr)oxides	Inherent N	SA-M/CN (M = Fe, Co, Ni, Mn, FeCo, FeNi)	0.9	Fe–N_4	Hydroxylation of benzene to phenol	78
	Metal phthalocyanine (MPc)	—	MPc@DNHCS-T (M = Fe, Co, Ni)	0.63–0.77	Co–N_4	CO_2 electroreduction and Zn–CO_2 batteries	218
	$Ni(acac)_2$	—	Ni SACs/N–C	0.1	Ni–N_4	Electrochemical oxidation of NO	215
	$FeCl_3$	—	Fe–N–C	0.3	Fe–N_4	ORR	82
	Metal acetylacetonates	—	M-ISAS/p-CN (M = Co, Ni, Cu, Mn, Pd, *etc.*)	0.42	M–N_4	ORR	217
	Metal nitrates	$Na_2WO_4·2H_2O$	WC_x–M (M = Fe, Ni, FeNi)	0.62–1.64	M–WC_x	OER	38
AAJ	Inherent Fe	Inherent N	Fe-ISA/NC	0.10	Fe–N_4	ORR	55
	Metal nitrates	Melamine	A-M/r-GO (M = Co, Zn, Cu, Ni)	3.6	Co–N_3C	ORR/Zn–air batteries	226

Table 2 (*continued*)

Biomass	Metal source	Heteroatom source	SACs	Loading (wt%)	Configuration	Catalytic application	Ref.
Sodium alginate	$FeCl_3$	Melamine	FeNC	0.4	$Fe–N_4$	ORR/Zn–air batteries	225
Porphyra	Iron phthalocyanine (FePc)	Inherent amino acids	$Fe–N_x$/HPC	0.35	$Fe–N_x$	ORR	227
	$FeCl_3·6H_2O$	—	Fe–NSDC	0.32	$Fe–N_3S$	ORR/OER/Zn–air batteries	228
	Natural hemin	—	SA-Fe/NHPC	0.48	$Cl–Fe–N_4$	ORR	222
	$PtCl_4$, inherent Fe	Urea	Fe_1Pt_1/NC	0.166, 2.29	$Fe–N_4$, $Pt–N_4$	ORR/HER	229
Enteromorpha	Inherent Fe	Inherent N	Fe–N–C	0.84	$Fe–N_2O_2$	PMS-driven organics degradation	53
	Inherent Fe	Inherent N	Fe–N@C	0.60	$Fe–N_x$	PMS-driven organics degradation	52
	$Fe(NO_3)_3$	Melamine	FeSA-NEPBC	1.3	$Fe–N_4$	Peroxydisulfate (PDS)-driven organics degradation	231
Microalgae	$Co(NO_3)_2·6H_2O$	Inherent amino groups	Co–N/C-SAC	3.1	$Co–N_4$	ORR	35
	Endogenous metals	$g\text{-}C_3N_4$	malg-SACs	1.98	$Fe–N_4$	ORR/Zn–air batteries	223
	$MnCl_2·6H_2O$	Dicyandiamide	SA-Mn-NSC	7.6	$Mn–N_4$	PMS-driven organics degradation	236
	Inherent Fe	$g\text{-}C_3N_4$, inherent S	Fe_{SA}/FeO_{NC}/NSC	0.25	$Fe–N_4$	ORR/Zn–air batteries	54
Bacteria	Inherent Fe, metal salts (M^{n+} = Ir, Ru, Pt, Cu, or Pd)	—	SA-M (M = Fe, Ir, Pt, Ru, Cu, or Pd)	1	$M–N_3$, $Fe–N_4$, M–Fe	HER/OER	88
	$Co(SO_4)_3·7H_2O$, $Fe_2(SO_4)_3·10H_2O$	Oxygen groups	Fe–Co SAs	0.10–0.22, 0.08–0.19	$Fe–O_3$, $Co–O_3$, Fe–Co	Nitrogen reduction reaction (NRR)	239

Natural biomass resources can open a new pathway for improving the stability of CS-SACs from their intrinsic structural and functional elements. Typically, the hard biomass can provide carbonaceous structures with abundant storage sites for metal species and fast transport paths for electrolyte ions *via* the regularly arranged fibers or stacked layers. The channels or porous structures increase the specific surface areas for active center exposure for both metal binding and mass transfer during catalysis. Purity is the first key factor to realize control of the structures and properties in prepared SACs. Biomass carbonaceous precursors contain versatile components, where activation by thermal treatment or chemical reagents enables the full exposure of the surface for active center attachments. However, their main drawback is the removal of the impurities generated during activation. Energy consumption is also a concern in green development.

Although biomass has been employed to fabricate abundant, low-cost, and highly porous CS-SACs to date, further research on the preparation of biomass-derived CS-SACs is still urgently needed to drive advancements across various applications.

(1) Biomass waste has been largely disposed of by landfills annually, where being a precursor for CS-SACs can facilitate the full advantages of its utilization. At present, a few types of biomass waste materials, such as corn silk, spent coffee grounds, waste paper, pig liver, and blood, have been reported to fabricate CS-SACs and can affect the ultimate structural morphology. Fibrous and lamellar structures are easily obtained from bamboo and wood after their simple pre-treatment with alkaline solutions. These structures provide improved specific surface area for single-atom attachment. Furthermore, plant-derived biomass possess advantages in constructing SACs with macroscopic shapes for large-scale catalytic applications. Protein-sourced biomass such as silks and hairs possess fibrous structures but are much shorter in length compared with cellulose-based biomass, which can undergo structure inheritance carbonization to preserve their high aspect ratio morphologies at the microscale. The restructuring strategy involves the decomposition of precursors into small parts or dissolution into molecular chains, providing chances to shape the precursors and ultimate carbonaceous structures into multiple morphologies for versatile applications such as microspheres, tubes, aerogels, and sponge-like networks.

(2) Despite the abundant biomass resources on Earth, most of the current research is still limited to the lab-scale. The high-temperature carbonization with high levels of energy consumption dominates the conventional preparation of biomass-derived CS-SACs, which is a major concern for future sustainability. Thus, to realize the industrialization of biomass-derived CS-SACs, less energy input is necessary and demanded. Deep exploration of the inherent capabilities of certain living biomass organisms for SAC preparation can potentially serve as alternatives to conventional carbonization methods. Using the extracellular electron transfer (EET) pathway of bacteria is a typical representation. The electroactive bacterium GS[88] possesses a surface network of multiheme. Oxidation reactions occur in their cytoplasm and the electrons are transferred to the acceptors (*e.g.*, metal ions) located outside their cells to afford reduced single atoms, which are further fixed and stabilized by

the surface cytochromes. This highly efficient and green strategy has the potential to achieve industrialization in the future.

(3) Biomass-derived CS-SACs have attracted significant research attention in electrocatalysis, photocatalysis, and advanced oxidation processes. Thus, novel applications of these SACs are essential and promising to be explored. Enzymes are highly efficient and specific catalysts for bioreactions, where the enzyme-mimic characteristics of SACs show potential in biomedical applications, such as cancer therapy, antibacterial therapy, biosensing, oxidative-stress cytoprotection, and sepsis management. Biomass-derived precursors possess intrinsic biosafety, paving the way for their translation into medical devices or agents for bioreactions both *in vitro* and *in vivo*.

(4) Most CS-SACs derived from biomass primarily focus on the M–N_x–C sites, with limited research attention devoted to metal sites coordinated with other heteroatoms such as S, O, P, and B. Although the direct doping of heteroatoms in the biomass organism may appear uncomplicated, it often results in an unpredictable heteroatom doping content and an unclear doping mechanism. Some natural biomass-derived chemicals (*e.g.*, polyphenol) possess well-defined chemical structures and abundant functional groups, making heteroatom groups easier to modify, and thus should be worthy of further development in the future.

(5) At present, there is still a lack of universal calculations to predict the composition, relative content of diverse biomass materials and components, synthesis conditions, and physicochemical properties of the resulting carbon materials (*e.g.*, element type and functional groups). Consequently, obtaining ideal CS-SACs from biomass resources in a timely and precise manner remains a challenge. Incorporating machine learning techniques will further advance the systematic design and precise fabrication of biomass-derived CS-SACs. Although there have been some reports on the relationship between SAC structures and their corresponding applications, systematic information and analysis integrating the biomass types, carbon support structure, metal coordination configuration, carbonization conditions, and performance are still missing. We obtained qualitative evaluation on biomass and its derived SACs and collecting more detailed information will assist our understanding on the semi-quantitative and quantitative levels. Consequently, relevant information about biomass is effectively integrated, enabling the timely extraction of valuable insights to efficiently establish complex CS-SACs. It is essential to perform fundamental studies on the effects of the biomass chemical characteristics on the catalytic efficiency of CS-SACs. Finally, the employment of biomass waste may contribute to global waste minimization.

Conflicts of interest

The authors declare no competing interests.

Acknowledgements

We acknowledge financial support from the National Key R&D Program of China (2022YFA0912800), National Excellent Young Scientists Fund (00308054A1045), National Natural Science Foundation of China (22178233, 22108181), Talents Program of Sichuan Province, Double First-Class University Plan of Sichuan University, State Key Laboratory of Polymer Materials Engineering (sklpme 2020-03-01), Tianfu Emei Program of Sichuan Province (2022-EC02-00073-CG), Postdoctoral special funding of Sichuan Province (TB2022063) and the Postdoctoral Funding of Sichuan University (2022SCU12099).

Notes and references

1 H. Jiang, W. Yang, M. Xu, E. Wang, Y. Wei, W. Liu, X. Gu, L. Liu, Q. Chen, P. Zhai, X. Zou, P. M. Ajayan, W. Zhou and Y. Gong, *Nat. Commun.*, 2022, **13**, 6863.
2 J. Y. Liu, *ACS Catal.*, 2017, **7**, 34–59.
3 L. Minmin, W. Linlin, Z. Kangning, S. Shanshan, S. Qinsi, Z. Lei, S. Xueliang, Z. Yufeng and Z. Jiujun, *Energy Environ. Sci.*, 2019, **12**, 2890–2923.
4 G. Gao, Y. Jiao, E. R. Waclawik and A. Du, *J. Am. Chem. Soc.*, 2016, **138**, 6292–6297.
5 L. Lin, W. Zhou, R. Gao, S. Yao, X. Zhang, W. Xu, S. Zheng, Z. Jiang, Q. Yu, Y. W. Li, C. Shi, X. D. Wen and D. Ma, *Nature*, 2017, **544**, 80–83.
6 X. F. Yang, A. Wang, B. Qiao, J. Li, J. Liu and T. Zhang, *Acc. Chem. Res.*, 2013, **46**, 1740–1748.
7 J. Yang, B. Chen, X. Liu, W. Liu, Z. Li, J. Dong, W. Chen, W. Yan, T. Yao, X. Duan, Y. Wu and Y. Li, *Angew. Chem., Int. Ed.*, 2018, **57**, 9495–9500.
8 C. Zhu, S. Fu, Q. Shi, D. Du and Y. Lin, *Angew. Chem., Int. Ed.*, 2017, **56**, 13944–13960.
9 Y. C. Yao, S. L. Hu, W. X. Chen, Z. Q. Huang, W. C. Wei, T. Yao, R. R. Liu, K. T. Zang, X. Q. Wang, G. Wu, W. J. Yuan, T. W. Yuan, B. Q. Zhu, W. Liu, Z. J. Li, D. S. He, Z. G. Xue, Y. Wang, X. S. Zheng, J. C. Dong, C. R. Chang, Y. X. Chen, X. Hong, J. Luo, S. Q. Wei, W. X. Li, P. Strasser, Y. E. Wu and Y. D. Li, *Nat. Catal.*, 2019, **2**, 304–313.
10 L. N. Cao and J. L. Lu, *Catal. Sci. Technol.*, 2020, **10**, 2695–2710.
11 Y. F. Ma, X. H. Zhang, L. N. Cao and J. L. Lu, *Catal. Sci. Technol.*, 2021, **11**, 2844–2851.
12 Y. Y. Feng, Y. X. Guan, H. J. Zhang, Z. Y. Huang, J. Li, Z. Q. Jiang, X. Gu and Y. Wang, *J. Mater. Chem. A*, 2018, **6**, 11783–11789.
13 K. Jiang, M. Luo, M. Peng, Y. Q. Yu, Y. R. Lu, T. S. Chan, P. Liu, F. M. F. de Groot and Y. W. Tan, *Nat. Commun.*, 2020, **11**, 2701.
14 Q. M. Sun, N. Wang, T. J. Zhang, R. Bai, A. Mayoral, P. Zhang, Q. H. Zhang, O. Terasaki and J. H. Yu, *Angew. Chem., Int. Ed.*, 2019, **58**, 18570–18576.
15 Y. Hou, M. Qiu, M. G. Kim, P. Liu, G. T. Nam, T. Zhang, X. D. Zhuang, B. Yang, J. Cho, M. W. Chen, C. Yuan, L. C. Lei and X. L. Feng, *Nat. Commun.*, 2019, **10**, 1392.
16 M. M. Fan, J. W. Cui, J. J. Wu, R. Vajtai, D. P. Sun and P. M. Ajayan, *Small*, 2020, **16**, 1906782.
17 H. M. Zhang, W. H. Liu, D. Cao and D. J. Cheng, *iScience*, 2022, **25**, 104367.

18 Y. Chen, S. Ji, Y. Wang, J. Dong, W. Chen, Z. Li, R. Shen, L. Zheng, Z. Zhuang, D. Wang and Y. Li, *Angew. Chem., Int. Ed.*, 2017, **56**, 6937–6941.
19 K. Gao, B. Wang, L. Tao, B. V. Cunning, Z. Zhang, S. Wang, R. S. Ruoff and L. Qu, *Adv. Mater.*, 2019, **31**, 1805121.
20 A. K. Geim and K. S. Novoselov, *Nat. Mater.*, 2007, **6**, 183–191.
21 Y. C. Yang, Y. W. Yang, Z. X. Pei, K. H. Wu, C. H. Tan, H. Z. Wang, L. Wei, A. Mahmood, C. Yan, J. C. Dong, S. L. Zhao and Y. Chen, *Matter*, 2020, **3**, 1442–1476.
22 D. N. Zhou, X. Y. Li, H. S. Shang, F. J. Qin and W. X. Chen, *J. Mater. Chem. A*, 2021, **9**, 23382–23418.
23 C. Liu, H. Li, F. Liu, J. S. Chen, Z. X. Yu, Z. W. Yuan, C. J. Wang, H. L. Zheng, G. Henkelman, L. Wei and Y. Chen, *J. Am. Chem. Soc.*, 2020, **142**, 21861–21871.
24 H. Fei, J. Dong, M. J. Arellano-Jiménez, G. Ye, N. Dong Kim, E. L. Samuel, Z. Peng, Z. Zhu, F. Qin, J. Bao, M. J. Yacaman, P. M. Ajayan, D. Chen and J. M. Tour, *Nat. Commun.*, 2015, **6**, 8668.
25 H. B. Yang, S. F. Hung, S. Liu, K. D. Yuan, S. Miao, L. P. Zhang, X. Huang, H. Y. Wang, W. Z. Cai, R. Chen, J. J. Gao, X. F. Yang, W. Chen, Y. Q. Huang, H. M. Chen, C. M. Li, T. Zhang and B. Liu, *Nat. Energy*, 2018, **3**, 140–147.
26 X. Fu, P. Zamani, J. Y. Choi, F. M. Hassan, G. Jiang, D. C. Higgins, Y. Zhang, M. A. Hoque and Z. Chen, *Adv. Mater.*, 2017, **29**, 1604456.
27 X. X. Wang, D. A. Cullen, Y. T. Pan, S. Hwang, M. Wang, Z. Feng, J. Wang, M. H. Engelhard, H. Zhang, Y. He, Y. Shao, D. Su, K. L. More, J. S. Spendelow and G. Wu, *Adv. Mater.*, 2018, **30**, 1706758.
28 H. T. Chung, D. A. Cullen, D. Higgins, B. T. Sneed, E. F. Holby, K. L. More and P. Zelenay, *Science*, 2017, **357**, 479–484.
29 W. Q. Zhang, X. H. Qin, T. R. Wei, Q. Liu, J. Luo and X. J. Liu, *J. Colloid Interface Sci.*, 2023, **638**, 650–657.
30 S. Liu, M. M. Jin, J. Q. Sun, Y. J. Qin, S. S. Gao, Y. Chen, S. S. Zhang, J. Luo and X. J. Liu, *Chem. Eng. J.*, 2022, **437**, 135294.
31 X. He, Q. He, Y. Deng, M. Peng, H. Chen, Y. Zhang, S. Yao, M. Zhang, D. Xiao, D. Ma, B. Ge and H. Ji, *Nat. Commun.*, 2019, **10**, 3663.
32 Y. Wang, M. Zhang, X. Shen, H. Wang, H. Wang, K. Xia, Z. Yin and Y. Zhang, *Small*, 2021, **17**, 2008079.
33 H. He, R. Zhang, P. Zhang, P. Wang, N. Chen, B. Qian, L. Zhang, J. Yu and B. Dai, *Adv. Sci.*, 2023, **10**, 2205557.
34 M. B. Gawande, P. Fornasiero and R. Zboril, *ACS Catal.*, 2020, **10**, 2231–2259.
35 D. Wu, J. Hu, C. Zhu, J. Zhang, H. Jing, C. Hao and Y. Shi, *J. Colloid Interface Sci.*, 2021, **586**, 498–504.
36 H. Ejima, J. J. Richardson, K. Liang, J. P. Best, M. P. van Koeverden, G. K. Such, J. Cui and F. Caruso, *Science*, 2013, **341**, 154–157.
37 H. F. Wang, X. P. Li, Y. Jiang, M. H. Li, Q. Xiao, T. Zhao, S. Yang, C. H. Qi, P. P. Qiu, J. P. Yang, Z. Jiang and W. Luo, *Angew. Chem., Int. Ed.*, 2022, **61**, e202200465.
38 S. Li, B. Chen, Y. Wang, M. Y. Ye, P. A. van Aken, C. Cheng and A. Thomas, *Nat. Mater.*, 2021, **20**, 1240–1247.
39 Y. Q. Wang, B. Y. Yu, K. Liu, X. T. Yang, M. Liu, T. S. Chan, X. Q. Qiu, J. Li and W. Z. Li, *J. Mater. Chem. A*, 2020, **8**, 2131–2139.
40 T. Wu, S. Li, S. Liu, W. C. Cheong, C. Peng, K. Yao, Y. Li, J. Wang, B. Jiang and Z. Chen, *Nano Res.*, 2022, **15**, 3980–3990.
41 Z. Q. Lin, M. Escudero-Escribano and J. Li, *J. Mater. Chem. A*, 2022, **10**, 5670–5672.
42 N. C. Cheng, L. Zhang, K. Doyle-Davis and X. L. Sun, *Electrochem. Energy Rev.*, 2019, **2**, 539–573.
43 Y. J. Chen, S. F. Ji, C. Chen, Q. Peng, D. S. Wang and Y. D. Li, *Joule*, 2018, **2**, 1242–1264.
44 Y. Chen, J. Lin, B. H. Jia, X. D. Wang, S. Y. Jiang and T. Y. Ma, *Adv. Mater.*, 2022, **34**, 2201796.
45 L. Liu and A. Corma, *Chem. Rev.*, 2018, **118**, 4981–5079.
46 Q. Zhang and J. Guan, *Adv. Funct. Mater.*, 2020, **30**, 2000768.
47 Z. J. Li, D. H. Wang, Y. Wu and Y. D. Li, *Natl. Sci. Rev.*, 2018, **5**, 673–689.
48 L. W. Xing, Y. J. Jin, Y. X. Weng, R. Feng, Y. J. Ji, H. Y. Gao, X. Chen, X. W. Zhang, D. D. Jia and G. Wang, *Matter*, 2022, **5**, 788–807.
49 G. F. Liao, L. Zhang, C. X. Li, S. Y. Liu, B. Z. Fang and H. M. Yang, *Matter*, 2022, **5**, 3341–3374.
50 H. F. Xiong, A. K. Datye and Y. Wang, *Adv. Mater.*, 2021, **33**, 2004319.
51 W. J. Liu, H. Jiang and H. Q. Yu, *Chem. Rev.*, 2015, **115**, 12251–12285.
52 C. Chen, T. F. Ma, Y. N. Shang, B. Y. Gao, B. Jin, H. B. Dan, Q. Li, Q. Y. Yue, Y. W. Li, Y. Wang and X. Xu, *Appl. Catal., B*, 2019, **250**, 382–395.
53 L. Peng, X. G. Duan, Y. N. Shang, B. Y. Gao and X. Xu, *Appl. Catal., B*, 2021, **287**, 119963.
54 Y. Lei, F. W. Yang, H. M. Xie, Y. P. Lei, X. Y. Liu, Y. J. Si and H. H. Wang, *J. Mater. Chem. A*, 2020, **8**, 20629–20636.
55 X. L. Wang, J. Du, Q. H. Zhang, L. Gu, L. J. Cao and H. P. Liang, *Carbon*, 2020, **157**, 614–621.
56 Q. Yang, W. X. Wang, Y. Y. Zhou, J. C. Hao, G. D. Fang, C. Liu, P. X. Cui and Y. J. Wang, *ACS ES&T Engg*, 2023, **3**, 616–626.
57 X. Liang, N. H. Fu, S. C. Yao, Z. Li and Y. D. Li, *J. Am. Chem. Soc.*, 2022, **144**, 18155–18174.
58 Z. Pu, I. S. Amiinu, R. Cheng, P. Wang, C. Zhang, S. Mu, W. Zhao, F. Su, G. Zhang, S. Liao and S. Sun, *Nano-Micro Lett.*, 2020, **12**, 21.
59 H. Zhou, S. Hong, H. Zhang, Y. T. Chen, H. H. Xu, X. K. Wang, Z. Jiang, S. L. Chen and Y. Liu, *Appl. Catal., B*, 2019, **256**, 117767.
60 X. F. Liu, N. Fechler and M. Antonietti, *Chem. Soc. Rev.*, 2013, **42**, 8237–8265.
61 M. M. Zhang, K. X. Huang, Y. Ding, X. Y. Wang, Y. L. Gao, P. F. Li, Y. Zhou, Z. Guo, Y. Zhang and D. P. Wu, *Nanomaterials*, 2022, **12**, 4289.
62 D. Y. Wu, W. Liu, J. W. Hu, C. Zhu, H. Y. Jing, J. W. Zhang, C. Hao and Y. T. Shi, *Mater. Chem. Front.*, 2021, **5**, 3093–3098.
63 Y. Chen, Z. Li, Y. Zhu, D. Sun, X. Liu, L. Xu and Y. Tang, *Adv. Mater.*, 2019, **31**, 1806312.
64 N. N. Li, W. Liu, C. Zhu, C. Hao, J. Y. Guo, H. Y. Jing, J. W. Hu, C. C. Xin, D. Y. Wu and Y. T. Shi, *J. Energy Chem.*, 2021, **54**, 519–527.

65 M. Xiao, L. Zhang, B. Luo, M. Q. Lyu, Z. L. Wang, H. M. Huang, S. C. Wang, A. J. Du and L. Z. Wang, *Angew. Chem., Int. Ed.*, 2020, **59**, 7230–7234.
66 K. Wang, Z. J. Lu, J. Lei, Z. Y. Liu, Y. Z. Li and Y. L. Cao, *ACS Nano*, 2022, **16**, 11944–11956.
67 J. W. Hu, D. Y. Wu, C. Zhu, C. Hao, C. C. Xin, J. W. Zhang, J. Y. Guo, N. N. Li, G. F. Zhang and Y. T. Shi, *Nano Energy*, 2020, **72**, 104670.
68 W. Xia, J. Tang, J. Li, S. Zhang, K. C. Wu, J. He and Y. Yamauchi, *Angew. Chem., Int. Ed.*, 2019, **58**, 13354–13359.
69 J. Fu, Y. D. Hou, X. P. Liu, M. P. Zheng and M. K. Zhu, *J. Mater. Chem. C*, 2020, **8**, 8704–8731.
70 K. Zeng, J. Li, Y. P. Xie, H. P. Yang, X. Y. Yang, D. Zhong, W. X. Zhen, G. Flamant and H. P. Chen, *Energy*, 2020, **213**, 118801.
71 S. Frangini and A. Masi, *Int. J. Hydrogen Energy*, 2016, **41**, 18739–18746.
72 S. Raharjo, Y. Ueki, R. Yoshiie and I. Naruse, *Energy Fuels*, 2013, **27**, 2762–2766.
73 S. Frangini, *J. Power Sources*, 2008, **182**, 462–468.
74 Y. F. Chen, Z. J. Li, Y. B. Zhu, D. M. Sun, X. E. Liu, L. Xu and Y. W. Tang, *Adv. Mater.*, 2019, **31**, 1806312.
75 H. Zhang, Y. Liu, T. Chen, J. Zhang, J. Zhang and X. W. D. Lou, *Adv. Mater.*, 2019, **31**, 1904548.
76 C. Zhu, S. Fu, J. Song, Q. Shi, D. Su, M. H. Engelhard, X. Li, D. Xiao, D. Li, L. Estevez, D. Du and Y. Lin, *Small*, 2017, **13**, 1603407.
77 J. C. Li, F. Xiao, H. Zhong, T. Li, M. J. Xu, L. Ma, M. Cheng, D. Liu, S. Feng, Q. R. Shi, H. M. Cheng, C. Liu, D. Du, S. P. Beckman, X. Q. Pan, Y. H. Lin and M. H. Shao, *ACS Catal.*, 2019, **9**, 5929–5934.
78 M. L. Zhang, Y. G. Wang, W. X. Chen, J. C. Dong, L. R. Zheng, J. Luo, J. W. Wan, S. B. Tian, W. C. Cheong, D. S. Wang and Y. D. Li, *J. Am. Chem. Soc.*, 2017, **139**, 10976–10979.
79 Y. Z. Li, R. Cao, L. B. Li, X. N. Tang, T. L. Chu, B. Y. Huang, K. Yuan and Y. W. Chen, *Small*, 2020, **16**, 1906735.
80 T. He, B. Lu, Y. Chen, Y. Wang, Y. Zhang, J. L. Davenport, A. P. Chen, C. W. Pao, M. Liu, Z. Sun, A. Stram, A. Mordaunt, J. Velasco, Jr., Y. Ping, Y. Zhang and S. Chen, *Research*, 2019, **2019**, 6813585.
81 B. C. Hu, Z. Y. Wu, S. Q. Chu, H. W. Zhu, H. W. Liang, J. Zhang and S. H. Yu, *Energy Environ. Sci.*, 2018, **11**, 2208–2215.
82 L. B. Deng, L. Qiu, R. Hu, L. Yao, Z. J. Zheng, X. Z. Ren, Y. L. Li and C. X. He, *Appl. Catal., B*, 2022, **305**, 121058.
83 L. Jiao, R. Zhang, G. Wan, W. J. Yang, X. Wan, H. Zhou, J. L. Shui, S. H. Yu and H. L. Jiang, *Nat. Commun.*, 2020, **11**, 2831.
84 Y. J. Sa, D. J. Seo, J. Woo, J. T. Lim, J. Y. Cheon, S. Y. Yang, J. M. Lee, D. Kang, T. J. Shin, H. S. Shin, H. Y. Jeong, C. S. Kim, M. G. Kim, T. Y. Kim and S. H. Joo, *J. Am. Chem. Soc.*, 2016, **138**, 15046–15056.
85 M. Liu, J. J. Liu, Y. Song, Z. L. Li and F. Wang, *Appl. Catal., A*, 2019, **583**, 117120.
86 Y. T. Qu, L. G. Wang, Z. J. Li, P. Li, Q. H. Zhang, Y. Lin, F. Y. Zhou, H. J. Wang, Z. K. Yang, Y. D. Hu, M. Z. Zhu, X. Y. Zhao, X. Han, C. M. Wang, Q. Xu, L. Gu, J. Luo, L. R. Zheng and Y. E. Wu, *Adv. Mater.*, 2019, **31**, 1904496.
87 R. Ma, X. Cui, Y. L. Wang, Z. Y. Xiao, R. Luo, L. K. Gao, Z. N. Wei and Y. K. Yang, *J. Mater. Chem. A*, 2022, **10**, 5918–5924.
88 S. Pedireddy, R. Jimenez-Sandoval, M. K. Ravva, C. Nayak, D. H. Anjum, S. N. Jha, K. P. Katuri and P. E. Saikaly, *Adv. Funct. Mater.*, 2021, **31**, 2010916.
89 Y. N. Shang, X. G. Duan, S. B. Wang, Q. Y. Yue, B. Y. Gao and X. Xu, *Chin. Chem. Lett.*, 2022, **33**, 663–673.
90 L. Y. Hu, W. R. Li, L. Wang and B. Wang, *EnergyChem*, 2021, **3**, 100056.
91 Y. N. Shang, X. Xu, B. Y. Gao, S. B. Wang and X. G. Duan, *Chem. Soc. Rev.*, 2021, **50**, 5281–5322.
92 S. H. Ho, Y. D. Chen, R. X. Li, C. F. Zhang, Y. M. Ge, G. L. Cao, M. Ma, X. G. Duan, S. B. Wang and N. Q. Ren, *Water Res.*, 2019, **159**, 77–86.
93 Z. H. Wan, Y. Q. Sun, D. C. W. Tsang, E. Khan, A. C. K. Yip, Y. H. Ng, J. Rinklebe and Y. S. Ok, *Chem. Eng. J.*, 2020, **401**, 126136.
94 J. Shan, C. Ye, Y. Jiang, M. Jaroniec, Y. Zheng and S. Z. Qiao, *Sci. Adv.*, 2022, **8**, eabo0762.
95 Q. H. Li, W. X. Chen, H. Xiao, Y. Gong, Z. Li, L. R. Zheng, X. S. Zheng, W. S. Yan, W. C. Cheong, R. A. Shen, N. H. Fu, L. Gu, Z. B. Zhuang, C. Chen, D. S. Wang, Q. Peng, J. Li and Y. D. Li, *Adv. Mater.*, 2018, **30**, 1800588.
96 Y. D. Chen, Y. H. Yang, N. Q. Ren and X. G. Duan, *Curr. Opin. Chem. Eng.*, 2023, **41**, 100942.
97 W. Y. Du, Q. Z. Zhang, Y. N. Shang, W. Wang, Q. Li, Q. Y. Yue, B. Y. Gao and X. Xu, *Appl. Catal., B*, 2020, **262**, 118302.
98 Y. X. Wang, H. Y. Su, Y. H. He, L. G. Li, S. Q. Zhu, H. Shen, P. F. Xie, X. B. Fu, G. Y. Zhou, C. Feng, D. K. Zhao, F. Xiao, X. J. Zhu, Y. C. Zeng, M. H. Shao, S. W. Chen, G. Wu, J. Zeng and C. Wang, *Chem. Rev.*, 2020, **120**, 12217–12314.
99 W. X. Liu, J. X. Feng, T. R. Wei, Q. Liu, S. S. Zhang, Y. Luo, J. Luo and X. J. Liu, *Nano Res.*, 2023, **16**, 2325–2346.
100 C. Ye, N. Zhang, D. Wang and Y. Li, *Commun. Chem.*, 2020, **56**, 7687–7697.
101 B. S. Chang, S. L. Wu, Y. Wang, T. L. Sun and Z. Cheng, *Nanoscale Horiz.*, 2022, **7**, 1340–1387.
102 C. Gao, J. X. Low, R. Long, T. T. Kong, J. F. Zhu and Y. J. Xiong, *Chem. Rev.*, 2020, **120**, 12175–12216.
103 P. Qi, J. Wang, X. Djitcheu, D. H. He, H. M. Liu and Q. J. Zhang, *RSC Adv.*, 2021, **12**, 1216–1227.
104 J. Z. Li, C. Chen, L. K. Xu, Y. Zhang, W. Wei, E. R. Zhao, Y. Wu and C. Chen, *JACS Au*, 2023, **3**, 736–755.
105 G. Xing, M. Tong, P. Yu, L. Wang, G. Zhang, C. Tian and H. Fu, *Angew. Chem., Int. Ed.*, 2022, **61**, e202211098.
106 S. Zhou, K. Jin and M. J. Buehler, *Adv. Mater.*, 2021, **33**, 2003206.
107 W. Li, Z. Chen, H. Yu, J. Li and S. Liu, *Adv. Mater.*, 2021, **33**, 2000596.
108 H. Zhu, W. Luo, P. N. Ciesielski, Z. Fang, J. Y. Zhu, G. Henriksson, M. E. Himmel and L. Hu, *Chem. Rev.*, 2016, **116**, 9305–9374.

109 D. D. Li, Z. Han, K. Y. Leng, S. H. Ma, Y. Wang and J. B. Bai, *J. Mater. Sci.*, 2021, **56**, 12764–12774.
110 P. Wang, G. Zhang, X. Y. Wei, R. Liu, J. J. Gu and F. F. Cao, *J. Am. Chem. Soc.*, 2021, **143**, 3280–3283.
111 X. Peng, L. Zhang, Z. Chen, L. Zhong, D. Zhao, X. Chi, X. Zhao, L. Li, X. Lu, K. Leng, C. Liu, W. Liu, W. Tang and K. P. Loh, *Adv. Mater.*, 2019, **31**, 1900341.
112 L. X. Zhong, C. Y. Jiang, M. T. Zheng, X. W. Peng, T. C. Liu, S. B. Xi, X. Chi, Q. H. Zhang, L. Gu, S. Q. Zhang, G. Shi, L. Zhang, K. Z. Wu, Z. H. Chen, T. Z. Li, M. Dahbi, J. Alami, K. Amine and J. Lu, *ACS Energy Lett.*, 2021, **6**, 3624–3633.
113 H. Chang, H. Pan, F. Wang, Z. Zhang, Y. Kang and S. Min, *Nanoscale*, 2022, **14**, 10003–10008.
114 R. D. Reeves, A. J. M. Baker, T. Jaffré, P. D. Erskine, G. Echevarria and A. van der Ent, *New Phytol.*, 2018, **218**, 407–411.
115 N. Rascio and F. Navari-Izzo, *Plant Sci.*, 2011, **180**, 169–181.
116 J. F. Wang, Q. Y. Zhu, Y. G. Shan, Y. H. Wang, X. S. Song and X. H. Lei, *Geoderma*, 2018, **314**, 1–7.
117 J. T. Li, H. K. Gurajala, L. H. Wu, A. van der Ent, R. L. Qiu, A. J. M. Baker, Y. T. Tang, X. E. Yang and W. S. Shu, *Environ. Sci. Technol.*, 2018, **52**, 119801.
118 C. Liu, W. S. Liu, A. van der Ent, J. L. Morel, H. X. Zheng, G. B. Wang, Y. T. Tang and R. L. Qiu, *Chemosphere*, 2021, **282**, 131096.
119 Z. C. Liu, L. Z. Zhou, C. C. Gan, L. J. Hu, B. Pang, D. Zuo, G. Y. Wang, H. C. Wang and Y. L. Liu, *Ecotoxicol. Environ. Saf.*, 2023, **254**, 114757.
120 A. Sas-Nowosielska, R. Kucharski, E. Malkowski, M. Pogrzeba, J. M. Kuperberg and K. Krynski, *Environ. Pollut.*, 2004, **128**, 373–379.
121 D. F. Liu, Y. S. Liu, M. Y. Liu, Y. P. Geng, Y. J. Zhang, E. Siemann, B. Li and Y. Wang, *J. Pest Sci.*, 2023, **183**, DOI: **10.1007/s10340-023-01654-0**.
122 D. F. Liu, L. Chen, C. Chen, X. K. An, Y. J. Zhang, Y. Wang and Q. J. Li, *BMC Plant Biol.*, 2020, **20**, 396.
123 P. Cui, C. Liu, X. Su, Q. Yang, L. Ge, M. Huang, F. Dang, T. Wu and Y. Wang, *Environ. Sci. Technol.*, 2022, **56**, 8034–8042.
124 X. Guo, Q. Z. Mu, H. Zhong, P. Li, C. J. Zhang, D. Wei and T. K. Zhao, *Environ. Pollut.*, 2019, **254**, 113101.
125 J. Cui, W. Wang, J. F. Li, J. M. Du, Y. J. Chang, X. J. Liu, C. Hu, J. W. Cui, C. Liu and D. R. Yao, *Ecotoxicol. Environ. Saf.*, 2021, **213**, 112032.
126 H. Guo, J. W. Jiang, J. Q. Gao, J. S. Zhang, L. Y. Zeng, M. Cai and J. L. Zhang, *Ecotoxicol. Environ. Saf.*, 2020, **195**, 110502.
127 Z. Li, K. Li, S. Ma, B. Dang, Y. Li, H. Fu, J. Du and Q. Meng, *J. Colloid Interface Sci.*, 2021, **582**, 598–609.
128 X. Li, K. Hu, Y. Z. Huang, Q. Q. Gu, Y. W. Chen, B. Yang, R. L. Qiu, W. H. Luo, B. M. Weckhuysen and K. Yan, *J. Energy Chem.*, 2022, **69**, 282–291.
129 A. Saravanan, S. Karishma, P. S. Kumar and G. Rangasamy, *Fuel*, 2023, **338**, 127221.
130 D. M. C. Chen, B. L. Bodirsky, T. Krueger, A. Mishra and A. Popp, *Environ. Res. Lett.*, 2020, **15**, 074021.
131 S. Babu, S. S. Rathore, R. Singh, S. Kumar, V. K. Singh, S. K. Yadav, V. Yadav, R. Raj, D. Yadav, K. Shekhawat and O. A. Wani, *Bioresour. Technol.*, 2022, **360**, 127566.
132 P. Kaur, J. Singh, M. Kaur, P. Rasane, S. Kaur, J. Kaur, V. Nanda, C. M. Mehta and D. Sowdhanya, *Waste Biomass Valorization*, 2023, **14**, 1413–1432.
133 Y. L. Zhang, R. Zhao, Y. Q. Li, X. X. Zhu, B. Zhang, X. Y. Lang, L. J. Zhao, B. Jin, Y. F. Zhu and Q. Jiang, *J. Power Sources*, 2021, **481**, 228644.
134 Z. M. Zou, X. L. Luo, L. Wang, Y. Zhang, Z. J. Xu and C. H. Jiang, *J. Energy Storage*, 2021, **44**, 103385.
135 C. L. Jiao, Z. Xu, J. Z. Shao, Y. Xia, J. Tseng, G. Y. Ren, N. J. Zhang, P. F. Liu, C. X. Liu, G. S. Li, S. Chen, S. Q. Chen and H. L. Wang, *Adv. Funct. Mater.*, 2023, **33**, 2213897.
136 P. X. Cui, Q. Yang, C. Liu, Y. Wang, G. D. Fang, D. D. Dionysiou, T. L. Wu, Y. Y. Zhou, J. X. Ren, H. B. Hou and Y. J. Wang, *ACS ES&T Engg*, 2021, **1**, 1460–1469.
137 M. Y. Qian, M. C. Lu, M. J. Yan, C. F. Chen, Y. W. Hu, Y. Li, J. R. Chen and X. L. Wu, *J. Environ. Chem. Eng.*, 2023, **11**, 109219.
138 J. McNutt and Q. He, *J. Ind. Eng. Chem.*, 2019, **71**, 78–88.
139 A. Colantoni, E. Paris, L. Bianchini, S. Ferri, V. Marcantonio, M. Carnevale, A. Palma, V. Civitarese and F. Gallucci, *Sci. Rep.*, 2021, **11**, 5119.
140 R. Campos-Vega, G. Loarca-Pina, H. A. Vergara-Castaneda and B. D. Oomah, *Trends Food Sci. Technol.*, 2015, **45**, 24–36.
141 A. Kovalcik, S. Obruca and I. Marova, *Food Bioprod. Process.*, 2018, **110**, 104–119.
142 A. Cervera-Mata, A. Fernandez-Arteaga, M. Navarro-Alarcon, D. Hinojosa, S. Pastoriza, G. Delgado and J. A. Rufian-Henares, *J. Cleaner Prod.*, 2021, **328**, 129548.
143 V. Kumar, P. Pathak and N. K. Bhardwaj, *Waste Manage.*, 2020, **102**, 281–303.
144 Z. J. Ma, Y. Yang, W. Q. Chen, P. Wang, C. Wang, C. Zhang and J. B. Gan, *Environ. Sci. Technol.*, 2021, **55**, 8492–8501.
145 X. D. Tang, G. Ran, J. J. Li, Z. Q. Zhang and C. X. Xiang, *J. Hazard. Mater.*, 2021, **402**, 123579.
146 J. F. Yang, Z. F. Ao, H. Wu, S. F. Zhang, C. C. Chi, C. Hou and L. W. Qian, *Renewable Energy*, 2020, **146**, 477–483.
147 M. J. Amicucci, E. Nandita, A. G. Galermo, J. J. Castillo, S. Chen, D. Park, J. T. Smilowitz, J. B. German, D. A. Mills and C. B. Lebrilla, *Nat. Commun.*, 2020, **11**, 3963.
148 A. S. A. Mohammed, M. Naveed and N. Jost, *J. Polym. Environ.*, 2021, **29**, 2359–2371.
149 E. Nandita, N. P. Bacalzo, Jr., C. L. Ranque, M. J. Amicucci, A. Galermo and C. B. Lebrilla, *Carbohydr. Polym.*, 2021, **257**, 117570.
150 A. Apriyanto, J. Compart and J. Fettke, *Plant Sci.*, 2022, **318**, 111223.
151 T. Cai, H. B. Sun, J. Qiao, L. L. Zhu, F. Zhang, J. Zhang, Z. J. Tang, X. L. Wei, J. G. Yang, Q. Q. Yuan, W. Y. Wang, X. Yang, H. Y. Chu, Q. Wang, C. You, H. W. Ma, Y. X. Sun, Y. Li, C. Li, H. F. Jiang, Q. H. Wang and Y. H. Ma, *Science*, 2021, **373**, 1523–1527.
152 F. G. Torres, O. P. Troncoso, A. Pisani, F. Gatto and G. Bardi, *Int. J. Mol. Sci.*, 2019, **20**, 5092.
153 L. C. Huang, H. Y. Tan, C. Q. Zhang, Q. F. Li and Q. Q. Liu, *Plant Commun.*, 2021, **2**, 100237.
154 M. Q. Li, Z. H. Bi, L. J. Xie, G. H. Sun, Z. Liu, Q. Q. Kong, X. X. We and C. M. Chen, *ACS Sustainable Chem. Eng.*, 2019, **7**, 14796–14804.

155 J. H. Cao, C. Y. Zhu, Y. Aoki and H. Habazaki, *ACS Sustainable Chem. Eng.*, 2018, **6**, 7292–7303.
156 Y. Kim, J. K. Kim, C. Vaalma, G. H. Bae, G. T. Kim, S. Passerini and Y. Kim, *Carbon*, 2018, **129**, 564–571.
157 M. Shen, W. Hu, C. Duan, J. Li, S. Ding, L. Zhang, J. Zhu and Y. Ni, *J. Colloid Interface Sci.*, 2023, **629**, 778–785.
158 D. Li, F. Zhang, L. Luo, Y. W. Shang, S. S. Yang, J. X. Wang, W. X. Chen and Z. A. Liu, *Chem. Eng. J.*, 2023, **461**, 142104.
159 T. Li, C. J. Chen, A. H. Brozena, J. Y. Zhu, L. X. Xu, C. Driemeier, J. Q. Dai, O. J. Rojas, A. Isogai, L. Wagberg and L. B. Hu, *Nature*, 2021, **590**, 47–56.
160 A. Plucinski, Z. Lyu and B. Schmidt, *J. Mater. Chem. B*, 2021, **9**, 7030–7062.
161 D. C. Wang, H. Y. Yu, D. M. Qi, Y. H. Wu, L. M. Chen and Z. H. Li, *J. Am. Chem. Soc.*, 2021, **143**, 11620–11630.
162 L. J. Xie, C. Tang, M. X. Song, X. Q. Guo, X. M. Li, J. X. Li, C. Yan, Q. Q. Kong, G. H. Sun, Q. Zhang, F. Y. Su and C. M. Chen, *J. Energy Chem.*, 2022, **72**, 554–569.
163 S. Zhang, S. F. Jiang, B. C. Huang, X. C. Shen, W. J. Chen, T. P. Zhou, H. Y. Cheng, B. H. Cheng, C. Z. Wu, W. W. Li, H. Jiang and H. Q. Yu, *Nat. Sustainability*, 2020, **3**, 753–760.
164 X. Liu, Y. Pei, M. B. Cao, H. B. Yang and Y. S. Li, *Chem. Eng. J.*, 2022, **450**, 138194.
165 A. M. Chiorcea-Paquim, T. A. Enache, E. D. Gil and A. M. Oliveira-Brett, *Compr. Rev. Food Sci. Food Saf.*, 2020, **19**, 1680–1726.
166 S. Khoshnoudi-Nia, N. Sharif and S. M. Jafari, *Trends Food Sci. Technol.*, 2020, **95**, 59–74.
167 A. J. Ragauskas, G. T. Beckham, M. J. Biddy, R. Chandra, F. Chen, M. F. Davis, B. H. Davison, R. A. Dixon, P. Gilna, M. Keller, P. Langan, A. K. Naskar, J. N. Saddler, T. J. Tschaplinski, G. A. Tuskan and C. E. Wyman, *Science*, 2014, **344**, 1246843.
168 W. Zhang, J. Yin, C. Wang, L. Zhao, W. Jian, K. Lu, H. Lin, X. Qiu and H. N. Alshareef, *Small Methods*, 2021, **5**, 2100896.
169 J. C. del Rio, J. Rencoret, A. Gutierrez, T. Elder, H. Kim and J. Ralph, *ACS Sustainable Chem. Eng.*, 2020, **8**, 4997–5012.
170 S. C. Wang, J. X. Bai, M. T. Innocent, Q. Q. Wang, H. X. Xiang, J. G. Tang and M. F. Zhu, *Green Energy Environ.*, 2022, **7**, 578–605.
171 W. Zhang, X. Qiu, C. Wang, L. Zhong, F. Fu, J. Zhu, Z. Zhang, Y. Qin, D. Yang and C. C. Xu, *Carbon Res.*, 2022, **1**, 14.
172 H. Wang, P. Feng, F. Fu, X. Yu, D. Yang, W. Zhang, L. Niu and X. Qiu, *Carbon Neutralization*, 2022, **1**, 277–297.
173 J. Z. Qin, B. Han, X. M. Lu, J. B. Nie, C. S. Xian and Z. H. Zhang, *JACS Au*, 2023, **3**, 801–812.
174 Y. Ju, H. Liao, J. J. Richardson, J. Guo and F. Caruso, *Chem. Soc. Rev.*, 2022, **51**, 4287–4336.
175 X. Zhang, Z. Li, P. Yang, G. Duan, X. Liu, Z. Gu and Y. Li, *Mater. Horiz.*, 2021, **8**, 145–167.
176 J. Guo, T. Suma, J. J. Richardson and H. Ejima, *ACS Biomater. Sci. Eng.*, 2019, **5**, 5578–5596.
177 J. J. Zhou, Z. X. Lin, Y. Ju, M. A. Rahim, J. J. Richardson and F. Caruso, *Acc. Chem. Res.*, 2020, **53**, 1269–1278.
178 Q. Dai, H. M. Geng, Q. Yu, J. C. Hao and J. W. Cui, *Theranostics*, 2019, **9**, 3170–3190.
179 D. Wu, J. J. Zhou, M. N. Creyer, W. Yim, Z. Chen, P. B. Messersmith and J. V. Jokerst, *Chem. Soc. Rev.*, 2021, **50**, 4432–4483.
180 Z. Zhang, L. S. Xie, Y. Ju and Y. L. Dai, *Small*, 2021, **17**, 2100314.
181 H. Ejima, J. J. Richardson and F. Caruso, *Nano Today*, 2017, **12**, 136–148.
182 J. Pan, G. Gong, Q. Wang, J. Shang, Y. He, C. Catania, D. Birnbaum, Y. Li, Z. Jia, Y. Zhang, N. S. Joshi and J. Guo, *Nat. Commun.*, 2022, **13**, 2117.
183 J. Guo, Y. Ping, H. Ejima, K. Alt, M. Meissner, J. J. Richardson, Y. Yan, K. Peter, D. von Elverfeldt, C. E. Hagemeyer and F. Caruso, *Angew. Chem., Int. Ed.*, 2014, **53**, 5546–5551.
184 J. Guo, B. L. Tardy, A. J. Christofferson, Y. Dai, J. J. Richardson, W. Zhu, M. Hu, Y. Ju, J. Cui, R. R. Dagastine, I. Yarovsky and F. Caruso, *Nat. Nanotechnol.*, 2016, **11**, 1105–1111.
185 Y. Zhang, J. Wang, Y. He, J. Pan, X. Jin, J. Shang, G. Gong, J. J. Richardson, I. Manners and J. Guo, *Angew. Chem., Int. Ed.*, 2023, **62**, e202303463.
186 Z. Zhao, D. C. Pan, Q. M. Qi, J. Kim, N. Kapate, T. Sun, C. W. Shields IV, L. L. Wang, D. Wu, C. J. Kwon, W. He, J. Guo and S. Mitragotri, *Adv. Mater.*, 2020, **32**, 2003492.
187 X. Liao, G. Gong, M. Dai, Z. Xiang, J. Pan, X. He, J. Shang, A. M. Blocki, Z. Zhao, C. W. T. Shields and J. Guo, *Adv. Sci.*, 2023, **10**, 2207488.
188 J. Guo, M. Suástegui, K. K. Sakimoto, V. M. Moody, G. Xiao, D. G. Nocera and N. S. Joshi, *Science*, 2018, **362**, 813–816.
189 X. Wei, D. Zheng, M. Zhao, H. Z. Chen, X. Fan, B. Gao, L. Gu, Y. Guo, J. B. Qin, J. Wei, Y. L. Zhao and G. C. Zhang, *Angew. Chem., Int. Ed.*, 2020, **59**, 14639–14646.
190 H. S. Kim, J. Lee, J. H. Jang, H. Jin, V. K. Paidi, S. H. Lee, K. S. Lee, P. Kim and S. J. Yoo, *Appl. Surf. Sci.*, 2021, **563**, 150208.
191 J. Lee, H. S. Kim, J. H. Jang, E. H. Lee, H. W. Jeong, K. S. Lee, P. Kim and S. J. Yoo, *ACS Sustainable Chem. Eng.*, 2021, **9**, 7863–7872.
192 Y. Zhu, W. Sun, J. Luo, W. Chen, T. Cao, L. Zheng, J. Dong, J. Zhang, M. Zhang, Y. Han, C. Chen, Q. Peng, D. Wang and Y. Li, *Nat. Commun.*, 2018, **9**, 3861.
193 Z. Y. Sun, Y. J. Wei, T. Cao, Z. Liu, R. Sui, X. Li, J. J. Pei, Z. Chen and S. Wang, *Nano Res.*, 2023, **16**, 9003–9011.
194 M. Borghei, J. Lehtonen, L. Liu and O. J. Rojas, *Adv. Mater.*, 2018, **30**, 1703691.
195 J. Zheng, C. Z. Guo, C. Y. Chen, M. Z. Fan, J. P. Gong, Y. F. Zhang, T. X. Zhao, Y. L. Sun, X. F. Xu, M. M. Li, R. Wang, Z. L. Luo and C. G. Chen, *Electrochim. Acta*, 2015, **168**, 386–393.
196 W. J. Jiang, W. L. Hu, Q. H. Zhang, T. T. Zhao, H. Luo, X. Zhang, L. Gu, J. S. Hu and L. J. Wan, *Chem. Commun.*, 2018, **54**, 1307–1310.
197 C. Y. Wang, X. Li, E. L. Gao, M. Q. Jian, K. L. Xia, Q. Wang, Z. P. Xu, T. L. Ren and Y. Y. Zhang, *Adv. Mater.*, 2016, **28**, 6640–6648.
198 C. Wang, W. Chen, K. Xia, N. Xie, H. Wang and Y. Zhang, *Small*, 2019, **15**, 1804966.

199 X. Y. Xu, J. Y. Wu, Z. H. Meng, Y. R. Li, Q. L. Huang, Y. Qi, Y. F. Liu, D. Zhan and X. Y. Liu, *ACS Appl. Nano Mater.*, 2018, **1**, 5460v5469.
200 H. Amiri, M. Aghbashlo, M. Sharma, J. Gaffey, L. Manning, S. M. M. Basri, J. F. Kennedy, V. K. Gupta and M. Tabatabaei, *Nat. Food*, 2022, **3**, 822–828.
201 H. Ababneh and B. H. Hameed, *Int. J. Biol. Macromol.*, 2021, **186**, 314–327.
202 A. Khan, M. Goepel, J. C. Colmenares and R. Glaser, *ACS Sustainable Chem. Eng.*, 2020, **8**, 4708–4727.
203 Y. Q. Zhu, W. M. Sun, W. X. Chen, T. Cao, Y. Xiong, J. Luo, J. C. Dong, L. R. Zheng, J. Zhang, X. L. Wang, C. Chen, Q. Peng, D. S. Wang and Y. D. Li, *Adv. Funct. Mater.*, 2018, **28**, 1802167.
204 Z. Liu, H. Li, X. Gao, X. Guo, S. Wang, Y. Fang and G. Song, *Nat. Commun.*, 2022, **13**, 4716.
205 G. Y. Zhang, X. Liu, L. Wang and H. G. Fu, *J. Mater. Chem. A*, 2022, **10**, 9277–9307.
206 W. X. Chen, J. J. Pei, C. T. He, J. W. Wan, H. L. Ren, Y. Q. Zhu, Y. Wang, J. C. Dong, S. B. Tian, W. C. Cheong, S. Q. Lu, L. R. Zheng, X. S. Zheng, W. S. Yan, Z. B. Zhuang, C. Chen, Q. Peng, D. S. Wang and Y. D. Li, *Angew. Chem., Int. Ed.*, 2017, **56**, 16086–16090.
207 Z. L. Wang, D. Xu, H. X. Zhong, J. Wang, F. L. Meng and X. B. Zhang, *Sci. Adv.*, 2015, **1**, e1400035.
208 N. Yang, R. Shao, Z. P. Zhang, M. L. Dou, J. Niu and F. Wang, *Carbon*, 2021, **178**, 775–782.
209 J. Alipal, N. A. S. M. Pu'ad, T. C. Lee, N. H. M. Nayan, N. Sahari, H. Basri, M. I. Idris and H. Z. Abdullah, *Mater. Today Proc.*, 2021, **42**, 240–250.
210 Y. Chen, T. He, Q. M. Liu, Y. F. Hu, H. Gu, L. Deng, H. T. Liu, Y. C. Liu, Y. N. Liu, Y. Zhang, S. W. Chen and X. P. Ouyang, *Appl. Catal., B*, 2023, **323**, 122163.
211 T. He, Y. Song, Y. Chen, X. Song, B. Lu, Q. Liu, H. Liu, Y. Zhang, X. Ouyang and S. Chen, *Chem. Eng. J.*, 2022, **442**, 136337.
212 J. A. Duce, S. Ayton, A. A. Miller, A. Tsatsanis, L. Q. Lam, L. Leone, J. E. Corbin, H. Butzkueven, T. J. Kilpatrick, J. T. Rogers, K. J. Barnham, D. I. Finkelstein and A. I. Bush, *Mol. Psychiatry*, 2013, **18**, 245–254.
213 H. Lee, S. M. Dellatore, W. M. Miller and P. B. Messersmith, *Science*, 2007, **318**, 426–430.
214 Y. Liu, K. Ai and L. Lu, *Chem. Rev.*, 2014, **114**, 5057–5115.
215 M. Zhou, Y. Jiang, G. Wang, W. Wu, W. Chen, P. Yu, Y. Lin, J. Mao and L. Mao, *Nat. Commun.*, 2020, **11**, 3188.
216 Y. Meng, P. Liu, W. Zhou, J. Ding and J. Liu, *ACS Nano*, 2018, **12**, 9070–9080.
217 A. J. Han, W. X. Chen, S. L. Zhang, M. L. Zhang, Y. H. Han, J. Zhang, S. F. Ji, L. R. Zheng, Y. Wang, L. Gu, C. Chen, Q. Peng, D. S. Wang and Y. D. Li, *Adv. Mater.*, 2018, **30**, 1706508.
218 S. H. Gong, W. B. Wang, C. N. Zhang, M. H. Zhu, R. Q. Lu, J. J. Ye, H. Yang, C. D. Wu, J. Liu, D. W. Rao, S. Y. Shao and X. M. Lv, *Adv. Funct. Mater.*, 2022, **32**, 2110649.
219 X. L. Qi, Y. J. Huang, S. Y. You, Y. J. Xiang, E. Y. Cai, R. T. Mao, W. H. Pan, X. Q. Tong, W. Dong, F. F. Ye and J. L. Shen, *Adv. Sci.*, 2022, 2106015.
220 E. C. Liu, Y. Ji, F. Zhang, B. J. Liu and X. H. Meng, *J. Agric. Food Chem.*, 2021, **69**, 1739–1750.
221 Y. H. Zhao, L. Wang, D. S. Zhang, R. Li, T. Y. Cheng, Y. B. Zhang, X. J. Liu, G. Wong, Y. G. Tang, H. Wang and S. Gao, *Sci. Rep.*, 2019, **9**, 78.
222 Z. Zhang, X. Gao, M. Dou, J. Ji and F. Wang, *Small*, 2017, **13**, 1604290.
223 L. L. Ma, X. Hu, Y. Min, X. Y. Zhang, W. J. Liu, P. K. S. Lam, M. M. Jung, R. J. Zeng and R. Q. Ye, *Carbon*, 2023, **203**, 827–834.
224 D. H. Li, D. J. Yang, X. F. Yang, Y. Wang, Z. Q. Guo, Y. Z. Xia, S. L. Sun and S. J. Guo, *Angew. Chem., Int. Ed.*, 2016, **55**, 15925–15928.
225 R. Hao, S. Gu, J. J. Chen, Z. Y. Wang, Q. M. Gan, Z. Q. Wang, Y. P. Huang, P. G. Liu, K. L. Zhang, K. Y. Liu, C. Liu and Z. G. Lu, *Mater. Today Energy*, 2021, **21**, 100826.
226 L. J. Zhang, T. C. Liu, N. Chen, Y. Jia, R. S. Cai, W. Theis, X. F. Yang, Y. Z. Xia, D. J. Yang and X. D. Yao, *J. Mater. Chem. A*, 2018, **6**, 18417–18425.
227 Z. P. Zhang, X. J. Gao, M. L. Dou, J. Ji and F. Wang, *J. Mater. Chem. A*, 2017, **5**, 1526–1532.
228 J. Zhang, M. Zhang, Y. Zeng, J. Chen, L. Qiu, H. Zhou, C. Sun, Y. Yu, C. Zhu and Z. Zhu, *Small*, 2019, **15**, 1900307.
229 L. J. Cao, X. L. Wang, C. Yang, J. J. Lu, X. Y. Shi, H. W. Zhu and H. P. Liang, *ACS Sustainable Chem. Eng.*, 2021, **9**, 189–196.
230 B. Su, B. D. Ge, M. Z. Li, Y. Y. Chen, Y. M. Chen, J. H. Zhang, H. Chen and J. H. Li, *Fuel*, 2019, **237**, 763–768.
231 Z. J. Wang, J. G. Bao, H. Z. He, S. Mukherji, L. T. Luo and J. K. Du, *Chem. Eng. J.*, 2023, **458**, 141513.
232 N. E. A. El-Naggar, M. H. Hussein, S. A. Shaaban-Dessuuki and S. R. Dalal, *Sci. Rep.*, 2020, **10**, 3011.
233 X. F. Shen, J. J. Liu, F. F. Chu, P. K. S. Lam and R. J. Zeng, *Appl. Energy*, 2015, **158**, 348–354.
234 X. Hu, L. L. Ma, W. J. Liu, H. C. Li, M. M. Ma and H. Q. Yu, *Sci. Total Environ.*, 2021, **782**, 146844.
235 F. M. Morsy, *Photochem. Photobiol.*, 2011, **87**, 137–142.
236 C. Zhou, Y. Liang, W. Xia, E. Almatrafi, B. Song, Z. Wang, Y. Zeng, Y. Yang, Y. Shang, C. Wang and G. Zeng, *J. Hazard. Mater.*, 2023, **441**, 129871.
237 K. Richter, M. Schicklberger and J. Gescher, *Appl. Environ. Microbiol.*, 2012, **78**, 913–921.
238 S. Kalathil, K. P. Katuri, A. S. Alazmi, S. Pedireddy, N. Kornienko, P. Costa and P. E. Saikaly, *Chem. Mater.*, 2019, **31**, 3686–3693.
239 S. B. Zhang, M. M. Han, T. F. Shi, H. M. Zhang, Y. Lin, X. S. Zheng, L. R. Zheng, H. J. Zhou, C. Chen, Y. X. Zhang, G. Z. Wang, H. J. Yin and H. J. Zhao, *Nat. Sustainability*, 2023, **6**, 169–179.